ABSTRACT

Title of dissertation: DISTRIBUTED OPTIMIZATION OF RESOURCE ALLOCATION FOR SEARCH AND TRACK ASSIGNMENT WITH MULTIFUNCTION RADARS

Tracie A. Severson, Doctor of Philosophy, 2013

Dissertation directed by: Dr. Derek A. Paley
Department of Aerospace Engineering
and the Institute for Systems Research

The long-term goal of this research is to contribute to the design of a conceptual architecture and framework for the distributed coordination of multifunction radar systems. The specific research objective of this dissertation is to apply results from graph theory, probabilistic optimization, and consensus control to the problem of distributed optimization of resource allocation for multifunction radars coordinating on their search and track assignments. For multiple radars communicating on a radar network, cooperation and agreement on a network resource management strategy increases the group's collective search and track capability as compared to non-cooperative radars. Existing resource management approaches for a single multifunction radar optimize the radar's configuration by modifying the radar waveform and beam-pattern. Also, multi-radar approaches implement a top-down, centralized sensor management framework that relies on fused sensor data, which may be impractical due to bandwidth constraints.

This dissertation presents a distributed radar resource optimization approach for a network of multifunction radars. Linear and nonlinear models estimate the resource allocation for multifunction radar search and track functions. Interactions between radars occur over time-invariant balanced graphs that may be directed or undirected. The collective search area and target-assignment solution for coordinated radars is optimized by balancing resource usage across the radar network and minimizing total resource usage. Agreement on the global optimal target-assignment

solution is ensured using a distributed binary consensus algorithm. Monte Carlo simulations validate the coordinated approach over uncoordinated alternatives.

DISTRIBUTED OPTIMIZATION OF RESOURCE ALLOCATION FOR SEARCH AND TRACK ASSIGNMENT WITH MULTIFUNCTION RADARS

by

Tracie Andrusiak Severson

Dissertation submitted to the Faculty of the Graduate School of the
University of Maryland, College Park in partial fulfillment
of the requirements for the degree of
Doctor of Philosophy
2013

Advisory Committee:
Professor Derek A. Paley, Chair/Advisor
Professor David L. Akin
Professor Balakumar Balachandran, Dean's Representative
Professor Robert M. Sanner
Professor Raymond J. Sedwick

Dedication

To Matt and Luke

Acknowledgments

There are many individuals to whom I owe a debt of gratitude for their support and encouragement during the process of obtaining my Ph.D.

I sincerely thank my advisor, Dr. Derek Paley for giving me the opportunity to be a graduate student in his laboratory. He was willing to work within the time constraints imposed by my Navy Permanent Military Professor program as well as my personal research interests and for that I'm extremely grateful. In addition to teaching me invaluable skills in effective written communication and rigorous attention to detail in my research, Derek has taught me the importance of balancing professional aspirations with family commitments.

A heartfelt thank you to my former advisor at the University of Michigan, Dr. Dennis Bernstein. I'm excited that our paths have crossed once again after 13 years. I'm grateful to a number of students in the Collective Dynamics and Control Laboratory. I thank my officemate Levi DeVries for insightful discussions on everything from cooperative control to crop dusting. To Amanda Chicoli, Nitin Sydney, Frank Lagor, and Daigo Shishika—thank you for your friendship and encouragement. I've truly enjoyed getting to know you all. Thanks also to former CDCL member Cammy Peterson for her time and invaluable feedback.

The Navy has been my "home away from home" every since I graduated from high school. There are many mentors and friends who have played a key role in my Naval career and especially those who have helped me get to where I am today. I especially wish to thank RADM (Ret.) Brad Hicks, CAPT (Ret.) Albert Grecco,

CAPT Tim Kelly, CAPT (Ret.) Ronald Crowell, and CAPT Jim Kilby. I hope to one day exhibit half of the leadership abilities each of you possesses.

My faith, family, and friendships are the bedrock of my support group. To my dear friends — thank you for giving me the much needed distractions these past three years. I truly appreciate your genuine interest in my work and even more so your efforts to get me to away from my computer and outside to breathe in the fresh air. I thank my parents Gary and Karen for instilling in both their daughters a sense of integrity and a work ethic that drives us to complete each task we set our hearts upon. I am truly blessed to call you Mom and Dad. To my in-laws Ray and Roxie—your kindness and generosity humble me. A special thank you to my sister Ericka who always understood me before I even spoke.

Without the enduring love and support of my husband Matt and son Luke I would not have been able to complete this journey. Your sacrifices never went unnoticed. Thank you for making me feel like the best wife and mother even on days I had little to offer. I dedicate this dissertation to you.

Lastly I thank God for making all things possible and for always being in control!

This work was partially funded by the Office of Naval Research under Grant No. N00174-09-2-00023.

Table of Contents

List of Tables

List of Figures

Nomenclature

A_e	Effective antenna area
F	Motion model
G	Radar gain
G	Graph
H	Measurement model
L	Graph Laplacian
L_s	Radar system losses
M_k	Total number of targets tracked by radar k
P_{avg}	Average radar transmitter power
P_D	Probability of detection
P_{FA}	Probability of false alarm
P_k	Total normalized resource usage for radar k
P_t	Peak radar transmitter power
R	Measurement error covariance
S_k	Total number of search sectors for radar k
T	Radar scan time ($T = t(n+1) - t(n)$)
T_0	Standard temperature
T_{com}	Communication latency
TU	Track uncertainty
$X_m(n)$	State of target m at time step n
$Z_m(n)$	Measurement of target m at time step n
k	Radar index
m	Target index, $m \in \{1, ..., M_k\}$
n	Time index, $n = 1, 2, ...$
s	Search sector index, $s \in \{1, ..., S_k\}$
Ω	Search sector solid angle
$\Sigma_m^k(n)$	Error covariance matrix when radar k is tracking target m at time step n
δ	Distance between shipboard radars
κ	Boltzmann's constant
λ	Wavelength
ϕ	Elevation angle
ρ	Range
ρ_{un}	Maximum unambiguous range
σ	Radar cross section
θ	Azimuth angle

Chapter 1

Introduction

On July 5th, 2006, The Democratic People's Republic of Korea (DPRK or North Korea) reportedly fired at least seven separate ballistic missiles in two rounds of missile tests [1]. These included one long-range missile and (multiple) short-range missiles. The long-range Taepodong-2 missile was estimated by United States intelligence agencies as having a potential range reaching as far as Alaska (although this missile failed after about 42 seconds of flight). In response to this test and to other ballistic missile threats, the United States is developing ground- and sea-based multifunction radar technology to detect and track ballistic missiles of all ranges—short, medium, intermediate and long [2]. One of the greatest benefits of a multifunction radar is its ability to simultaneously perform search and track functions that previously required two or more radars. These functions can be executed rapidly and independently of one another to support a variety of mission requirements, such as missile early warning, data collection, and target engagement support [3],[4]. To facilitate the radar's ability to manage both its search and track tasking simultaneously, the radar resource manager must be able to dynamically vary the radar resource allocation between search and track functions depending upon the mission objectives and priorities. When the number of targets greatly exceeds the number of radars (high threat density), the resources required to track

each target may exceed each radar's resource availability. In this situation, missed target detections and leakers (targets that are detected but not tracked due to unavailable resources) may occur, especially if the radars are unable to coordinate on their collective resource allocation.

This dissertation presents a distributed, radar resource optimization framework for the search and track assignment in a network of multifunction radars. Fig. 1.1 illustrates a canonical raid scenario considered in which multiple ship-based radars search for and track ballistic targets while also providing air-defense. This framework includes a physically representative radar model that performs ballistic missile surveillance and tracking while concurrently executing air-defense surveillance. When the radar resource allocation is coordinated across the radar network, each radar seeks the radar-to-target assignment solution that balances the resource usage across the network and minimizes the total resource usage; ultimately leading to a reduction in the number of targets that go untracked.

1.1 Problem Statement

In a high threat density, multiple raid environment, management of radar resources to support surveillance and target tracking is critical to maximizing the likelihood of defeating all threats that target defended areas. In the pre-mission planning stages, optimal allocation of limited radar resources may be achieved by assigning search and track tasking based on anticipated threat launch areas and projected impact locations. Once targets are launched, however, multiple radars

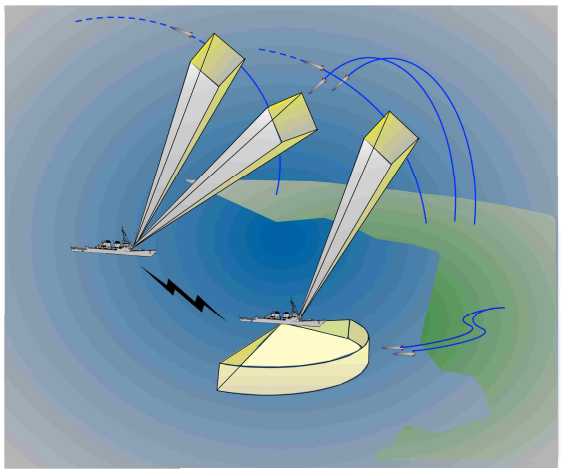

Figure 1.1: Multi-radar target tracking coordination in a ballistic missile (BM) and air-defense (AD) raid scenario.

may detect and track the same threat, reducing the limited available resources to search for and detect future targets [5]. While additional radar systems may alleviate some of the resource burden, a lack of coordination among the participating radars may still lead to untracked targets due to conflicting resource management priorities.

Cooperation and coordination among a network of mobile maritime multifunction radars has many advantages. One of the greatest advantages is the ability to dynamically allocate search and track tasking across the radar network [6],[7]. In military defense applications, tasking decisions are made so as to increase the collective probability of successfully processing all threats in a high threat density raid environment. Because resource usage is a function of the instantaneous search and track tasking, a resource allocation approach that optimizes the collective surveillance area while concurrently optimizing the radar-to-target assignment is needed. Balancing resource utilization across the radar network prevents a single radar from

using all of its available resources unless the other radars are also at or near their maximum capability. This is important if a majority of the threats are detected by a subset of radars. Equally important is minimizing the total resource usage among each radar, allowing for additional resources to be applied either to search or track functions, depending on the mission priorities as described in a resource allocation doctrine. Due to the potentially large number of targets, probabilistic approaches to solving the target-assignment problem, such as genetic algorithms, offer an alternative method to finding an optimal solution in a reduced timeframe [8].

Because the radars are mobile and often operate in adverse or communications-denied situations, the resource management framework must be robust to a dynamically changing threat environment that includes the addition or loss of radars to the network as well as limitations on communications and bandwidth availability. A consensus-based distributed (or decentralized) optimization approach allows each radar to reach agreement on the optimal target-assignment solution by repeatedly exchanging and updating their local target-assignment solutions in an iterative fashion that yields agreement on a single global solution. In multiagent networks, consensus means to reach an agreement on a state variable [9], which in our case is the radar-to-target assignments. A consensus algorithm is an interaction rule that specifies the information exchange between an agent and all of its neighbors on the network, typically represented by a graph [9]. Consensus algorithms are guaranteed to converge even under very mild assumptions on the communication network [10]; indeed, they are tolerant to time-varying, directed communication links [11] and time-delayed communication [12].

The three existing challenges to distributed optimization of resource management for multifunction radars addressed in this dissertation are as follows:

1. *Construction of a physically representative modeling framework of a multifunction radar mission that allows a group of radars to coordinate their surveillance and target-tracking functions.*

2. *Optimization of the radar resource allocation for a network of coordinated multifunction radars in a high threat density environment.*

3. *Demonstration through Monte Carlo simulations of the performance of the coordinated resource allocation approach verses uncoordinated alternatives.*

1.2 Relation to Previous Work

Radar sensing systems provide an attractive platform for sensor management applications due to their controllable degrees of freedom, such as bandwidth, frequency, sampling rate, and beamform. These characteristics, traditionally hardwired into the radar, now allow engineers to design and optimize their configuration to satisfy a variety of mission requirements by using a resource scheduling policy that accounts for the radar's resource constraints. One of the most well-developed focus applications of resource management for multifunction radar systems is the application of real-time, closed-loop scheduling of radar resources [13],[5]. Kershaw and Evans [14], [15] provided some of the earlier work on closed-loop waveform management for sensor management applications by investigating various adaptive waveform selection techniques based on single target tracking performance in white

Gaussian noise. Sowelam and Tewfix in [16], [17] study the radar management problem of adaptively selecting a minimal set of radar waveforms to obtain an accurate reconstruction of the target's reflectivity. Recent radar management approaches in the literature address radar waveform scheduling for reducing target angle accuracy [18],[19], target identification [20], target tracking [21], and estimating and tracking multiple targets [22]. In [23], an interleaving algorithm based on a Hopfield neural network is used to exploit the radar downtime (the time between transmitted and received pulses) to increase the number of tracking tasks. While optimizing the radar waveform scheduling seems extremely appropriate for a single radar platform or a multi-sensor system managed by a centralized controller with access to real-time information, its extension to multiple radars communicating over a distributed network presents some nontrivial challenges such as communication requirements and bandwidth limitations.

Single radar resource management approaches based on modeling the management as a decision process presented a new perspective and allowed engineers to apply the principles of Markov Decision Processes (MDP) and Partially Observed MDP (POMDP). Krishnamurthy [24] devised a radar management strategy to determine how much radar resource (time) to devote to each target based on a dynamic prioritization schema that accounts for the current target state estimates. Nino-Mora and Villar in [25] and La Scala and Moran in [26] formulate the resource management problem as a MDP and present a target update scheduling policy that assigns radar resources to reduce target tracking-error variances.

Myopic sensor management polices (i.e., policies that decide the best course of

action based upon an immediate reward) such as information-theoretic approaches, provide a lower complexity alternative to determine the optimal configuration for multifunction radar systems than policies that look ahead to a future reward. While future radar performance may be sacrificed by only considering its near-term state, in certain situations myopic scheduling policies may prove more robust to inaccurate sensor models and dynamic performance objectives. Khosla and Guillochon in [27] present an information-theoretic approach in which each target has a kinematic state and target class; sensors can observe either state or class (or both) depending upon which mode maximizes the information gained on the target. Sinno and Kreithen [28] present a cooperative surveillance and multi-target tracking optimization approach that maximizes the aggregate Signal-to-Noise Ratio (SNR) for all targets and minimizes target uncertainty. Kalandros and Pao in [29] use covariance control to determine the sensor(s) tracking resource allocation in order to reduce the target state uncertainty. Kreucher et al. in [30] present a sensor management scheme that maximizes the expected gain in information based on computing the Rényi Information Divergence [31].

Algorithms that utilize centralized planning nodes for multi-agent coordination demonstrate quicker search-area coverage and target neutralization than uncoordinated agents as described by Schumacher et.al in [32]. However restricted communications and processing resources pose significant challenges to a centralized sensor fusion center that receives and processes raw sensor data. When the expected target locations are unknown, optimization algorithms described by Smith and Bullo [33],[34] demonstrate detection of a group of distinct target locations

within a prescribed environment without assuming exact target coordinates.

For multiple ship-based radars considering a large number of targets, Kang and Lee [35] divide the radar search sectors such that the relative residual radar resource capacity is balanced and assign tracking responsibilities based on expected target arrivals to minimize target migrations from one ship's search sector to another ship's sector. While this approach preserves important target state information by minimizing migrations, it prevents a radar from tracking targets outside its own search sector, which may be beneficial in balancing the resource load; it also fails to address the situation when the tracking resources exceed resources available for search tasks. Distributed resource management approaches for several multifunction radars that combine resource minimization with information maximization are presented by Weir in [6] and Lambert and Sinno in [36] using emergent behavior and self-organization techniques.

1.3 Contributions of Dissertation

This dissertation applies results from graph theory, probabilistic optimization, and consensus control to the problem of distributed resource management for coordinated multifunction radars. Specific contributions are described below.

Multifunction radar system model Radar resource allocation is modeled using a physically representative, three-dimensional, nonlinear framework. Resources are consumed as each radar searches for, detects, and tracks ballistic missile (BM)

targets while concurrently executing air-defense (AD) surveillance requirements. Resources for engagements are modeled using an estimate of the resources required to reduce the track uncertainty to meet a prescribed engagement requirement.

Optimization of radar resource allocation A distributed approach optimizes both the collective surveillance area and radar-to-target assignment solution for multiple radars coordinating over a directed network. The radar-to-target-assignment problem for coordinated radars is solved by balancing radar resource usage and minimizing total radar resource utilization while simultaneously optimizing the limited search resources by maximizing the search area around the expected target arrival. The air defense strategy also maximizes the area of each radar's search sector, which is centered on an expected threat axis, and ensures that each search sector degrades symmetrically about the threat axis under heightened track demand.

Consensus-based coordination A distributed consensus algorithm reaches agreement on the single global target-assignment solution. The consensus algorithm provides robustness to inaccurate or unaccounted for sensor biases, eliminates the possibility that a detected target is untracked when tracking resources are available, and ensures that all radars share the same target-assignment solution even in the presence of communication noise.

Performance validation Monte Carlo simulations demonstrate that a decentralized consensus-based approach to reaching the global optimal radar-to-target as-

signment solution allows for a greater number of targets to be detected and tracked while preserving adequate resources for AD search. The coordinated approach described here permits each radar and its local resource manager to maintain control over its resource allocation subject to the consensus of the radar communication network. Results are compared to uncoordinated approaches using various existing resource allocation doctrines in order to highlight the increase in tracked targets and conservation of radar resources.

1.4 Outline of Dissertation

The outline of this dissertation is as follows.

Chapter 2 presents a physically-representative three-dimensional nonlinear model of a multifunction radar system, including models of radar detection, surveillance, target tracking, and target uncertainty. It reviews some fundamental properties of algebraic graph theory and consensus and describes their application to radar communication and target-assignment networks.

Chapter 3 applies a probabilistic optimization approach for maximizing the collective search-area of multiple radars coordinating over a directed network using simplified two-dimensional linear and nonlinear radar models as a first look at multi-radar resource management. The optimal target-assignment solution in the case of single or multiple targets in a linear resource usage model has target-assignment boundaries that are hyperbolic.

Chapter 4 describes an optimization framework for multiple three-dimensional

nonlinear radars coordinating over a strongly connected, balanced communication network with possibly directed links. Section 4.2 solves for the optimal radar-to-target-assignment, as represented by the adjacency matrix of the target assignment graph, using a binary genetic algorithm that balances radar resource tasking and minimizes total radar resource usage. Section 4.3 presents a distributed consensus-based approach for reaching agreement on the optimal target-assignment, adopting a binary consensus algorithm following [37] that is robust to communication noise and fading channels. The multifunction radar resource optimization approach is validated via Monte Carlo simulations in Section 4.4 and compared to two uncoordinated approaches for both a short range and medium range ballistic missile radar mission.

Chapter 5 summarizes the dissertation and provides suggestions for future research.

Chapter 2

Multifunction Radar Modeling Framework

A multifunction radar system performs a variety of functions originally assigned to multiple radars. Shipboard multifunction radars support surface search, air-defense search, ballistic missile search, ballistic missile tracking, and air-defense tracking [38]. Because the execution of each function is separable, the radar signal and data processing applied to each function can be controlled and optimized given the overall mission objectives [39]. While there are a variety of (oftentimes competing) objectives, the primary goal of this dissertation is to optimize the resource allocation for ballistic missile and air-defense search and track functions to increase the number of tracked ballistic missile targets.

This chapter presents the multifunction radar, communication, and target-assignment network models used in the multi-target search and track optimization approach. Section 2.1 reviews some fundamental properties of multifunction radar systems and resource management implementations, including the resource allocation doctrine. Section 2.2 introduces the search and track resource allocation models as well as the ballistic missile target kinematic model. Motivated by the radar's potential requirement to support a weapon's engagement, this section also describes a method to assess the performance of the target tracking system in terms of the track uncertainty and how this uncertainty estimate is incorporated in the radar re-

source model. Section 2.3 reviews some fundamental properties of graphs and their application to sensor networks and communication models including consensus.

2.1 Radar System Fundamentals

Radars operate by emitting electromagnetic energy in the form of an electromagnetic wave. Some of that energy is scattered due to the wave's interaction with the environment while a smaller portion of the scattered energy, called the radar echo, is collected by the receiving radar antenna (see Fig. 2.1). The time difference τ between when the pulse of electromagnetic energy is transmitted and when the target echo is received is proportional to the target range ρ, given by [4]

$$\tau = \frac{2\rho}{c}, \tag{2.1}$$

where c is the speed of the electromagnetic wave propagation. The pulse repetition interval (PRI) specifies the time interval between successive pulses and is inversely proportional to the pulse repetition frequency (PRF), where $PRF = 1/(PRI)$. Because of the time delay between when a radar pulse is transmitted and when the radar echo is received, range ambiguities may occur when it is not clear from which of the transmitted pulses the received echo originated. The maximum unambiguous range ρ_{un} is proportional to the pulse repetition interval, i.e., [38]

$$\rho_{un} = \frac{c(PRI)}{2}. \tag{2.2}$$

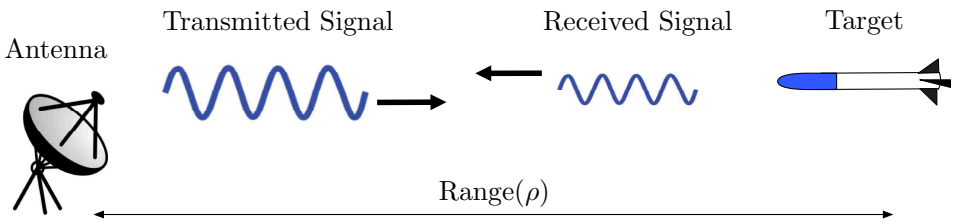

Figure 2.1: Received radar echo attenuated due to interaction with a target and the environment.

The duty cycle of a radar specifies the fraction of time that the radar system is in an "active" state, i.e., the portion of time the system is operational. The duty cycle is used to calculate both the peak power P_t and average power P_{avg} of a particular radar system, [4]

$$\text{Duty Cycle} = \frac{P_{avg}}{P_t}. \tag{2.3}$$

2.1.1 Detection Probability

A multifunction radar system produces range, doppler, and angle measurement data. In order to determine the presence of targets, signal processing is applied to the measurement data to differentiate between a target present hypothesis (H_1) and target not present hypothesis (H_0). Receiver background and thermal noise fluctuations complicates the decision process. The detection performance, Probability of Detection (P_D), depends upon the strength of the returned target signal relative to that of the noise (Signal to Noise Ratio) and threshold setting (Probability of False Alarm). The Neyman-Pearson criterion [40] says that the decision rule should be constructed to maximize the Probability of Detection while not allowing the

Probability of False Alarm to exceed a certain value,

$$max\{P_D\}, \text{ such that } P_{FA} \leq \alpha. \tag{2.4}$$

The solution to the optimization problem in 2.4 is given by the Neyman-Pearson lemma [41], which defines the optimal decision region for a fixed probability of false alarm P_{FA} as a threshold η on likelihood ratio LR for measurement vector X [39]:

$$LR(X) = \frac{p(X|H_1)}{p(X|H_0)} \underset{H_0}{\overset{H_1}{\gtrless}} \eta \tag{2.5}$$

where η is chosen such that $P_{FA} = p(X > \eta|H_0)$. For a minimum probability of detection and a maximum probability of false alarms, the Signal to Noise ratio (SNR) can be computed using Albersheim's equation [4], which provides a closed-form approximation of the SNR required for non-fluctuating targets in independent and identically distributed Gaussian noise (see Fig. 2.2).

2.1.2 Resource Allocation

Consider a network of identical multifunction radars that search for and track ballistic missiles (BM) while also performing air defense (AD) search. Each radar has the same maximum resource allocation and a fixed location. The initial resource allocation is partitioned into AD Search, AD Track, BM Search, BM Track, and Spare as shown in Fig. 2.3(a). As BM targets are detected and tracking assignments determined, BM Track consumes resources initially designated Spare to

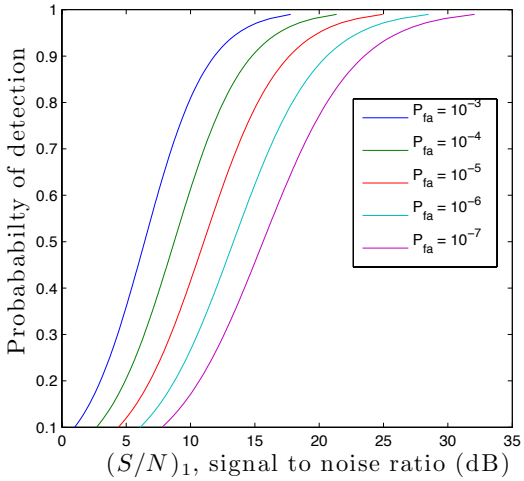

Figure 2.2: An increase in the SNR allows a greater detection probability for a smaller false alarm threshold.

track new targets as well as apportions BM tracking resources to reduce the target uncertainty of existing BM targets. These tracking resources are designated BM Track-Engage. Once all Spare resources are consumed by BM Track and BM Track-Engage, as depicted in Fig. 2.3(b), two possibilities exist: (i) additional BM targets are untracked and the resource allocation remains as shown in Fig. 2.3(b); or (ii) BM Track and BM Track-Engage consume additional resources initially reserved for AD Search as illustrated in Fig. 2.3(c) and the AD search sector is redefined. For case (ii), once AD search resources are fully consumed, no additional resources can be used for BM Track or BM Track-Engage, since AD Track is preserved.

In a multifunction radar network, the implementation of resource allocation for Search, Track, and Track-Engage resources can be done in a centralized framework or a decentralized (distributed) framework as shown in Fig 2.4. There are advantages and disadvantages to both implementations. In a centralized implemen-

tation, a central radar resource manager receives all search and track information from participating local resource managers and makes informed decisions based on global knowledge. These decisions are broadcast as directives to the local resource managers for execution and in theory should be optimal as compared to some performance objective based on full knowledge of the situation. The drawbacks to a

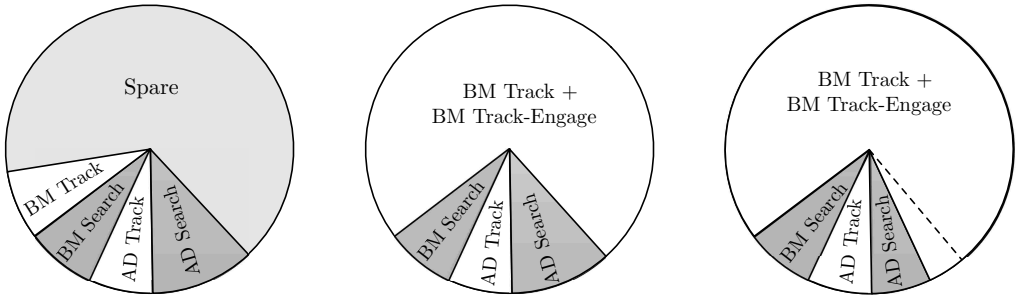

(a) Initial (b) Fixed (c) Variable

Figure 2.3: The radar resource manager will dynamically allocate finite available search and track resources to accomplish mission objectives and maximize system performance.

centralized implementation are the increased data exchange requirements between the local and central resource manager as well as a loss of local control at the radar level.

In contrast to a centralized resource management implementation, a distributed implementation allows each local radar resource manager to decide on the optimal resource management policy and then reach agreement on the global policy through the process of consensus. In this implementation, each local resource manager maintains control of their resource allocations subject to the consensus of the network. It also significantly reduces the information exchange requirements over an already bandwidth-constrained communication link.

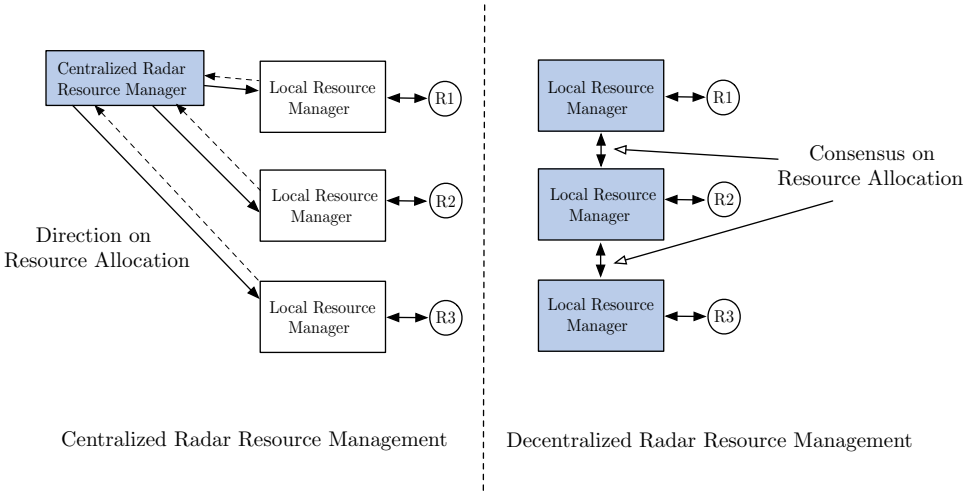

Figure 2.4: A centralized management implementation requires additional data exchanges and loss of local control whereas whereas a decentralized implementation reduces the communication requirements with a central server and allows for local resource control subject to the consensus of the network.

2.2 Multifunction Radar Model

2.2.1 Radar Search Function

Multifunction radars play a vital role in the defense against long and short range targets. The objective of the search function in a multifunction radar is to detect objects in a volume of space and to "acquire" them (i.e., initiate a target track) where they are then handed off to another radar function such as tracking [42]. While there are a number of different search types that radars can employ, the primary search types considered for ballistic missile defense are the volume and horizon searches [43].

Volume Search

A volume search is a 360° search patten [44] that covers the area around the sensor out to a defined range [44]. This type of search is used for radars operating in air defense applications such as the search and tracking of aircraft, cruise missiles, and UAVs where targets can originate from multiple directions. The downside of a volume search is the large amount of radar resources required to cover the full volume and therefore the relatively large amount of time to complete a search pattern. To reduce the time required to search the volume, the detection range can be reduced, however this impacts the long-range performance required for the ballistic missile defense mission [45].

To prevent range degradation for ballistic missile performance, a search sector is defined by its range, azimuth, and elevation, creating a volume search on a well-defined area. In addition to the characteristics above, a volume search is also specified by the time T_{search} required to execute the search, the allowed false-alarm rate P_{FA}, and the desired probability of detection P_D.

Horizon Search Fence

In contrast to a volumetric search, the horizon search utilizes only a single row of beams at or above the horizon for search and acquisition applications [42]. This search is commonly used for early warning missile surveillance radars as well as ballistic missile defense radars and operates under the assumption that for an adequate detection range, any ascending ballistic target must fly through the fence

and thus will be detected.

Resource Model

The Signal to Noise ratio (SNR) is the standard measure of a radar's ability to detect a given target at a range ρ from the radar [44]. SNR is a linear function of the inverse search sector solid angle[1] Ω and a quartic function of the inverse detection range ρ [4, pp. 30-90]:

$$\text{SNR} = \frac{P_{avg} A_e \sigma T_{search}}{4\pi\kappa T_0 L_s \rho^4 \Omega}, \tag{2.6}$$

where P_{avg} is the average transmitted power, A_e is the effective antenna area, σ is the target radar cross section, κ is Boltzmann's constant, T_0 is the radar system temperature, L_s are the total system losses, and T_{search} is the search scan time for solid angle Ω at range ρ. Radar resource usage is expressed in units of time by solving 2.6 for the search scan time T_{search}, which yields

$$T_{search} = a\rho^4\Omega, \tag{2.7}$$

where

$$a \triangleq 4\pi\kappa T_0(\text{SNR})L_s/(P_{avg}A_e\sigma) \tag{2.8}$$

is considered identical for all radars. To avoid unnecessary complexity, the radar model performs search tasks uniformly so that resources are equally distributed among each of the search directions in Ω.

[1]The solid angle subtended by a surface is the surface area of the portion of a unit sphere covered by the surface's radial projection onto the sphere [46].

For a particular radar system design and expected target surveillance mission, the parameters of 2.8 are assumed to be known and fixed. In the event of multiple search sectors, let S_k represent the total number of ballistic missile and air-defense search sectors for radar k. The total search scan time $T^{(tot)}_{search,k}$ dedicated to searching all S_k sectors of radar k is expressed as

$$T^{(tot)}_{search,k} = a \sum_{s=1}^{S_k} \rho^4_{s,k} \Omega_{s,k}, \tag{2.9}$$

where $s \in \{1, ..., S_k\}$ is the search sector index.

In many surveillance missions the potential threat axis is known (i.e., the most probable direction from which a target will arrive). The search sector is typically centered on this threat axis and its surface area maximized. Fig. 2.5 illustrates the geometry required for computing the surface area A and solid angle Ω. The surface area A of a spherical sector bounded by azimuth angles (θ_1, θ_2) and elevation angles (ϕ_1, ϕ_2) is

$$A = \rho^2(\theta_2 - \theta_1)(\cos\phi_2 - \cos\phi_1). \tag{2.10}$$

Dividing 2.10 by ρ^2 gives the solid angle [46] $\Omega = (\theta_2 - \theta_1)(\cos\phi_2 - \cos\phi_1)$.

The surface area in 2.10 is maximized along a potential threat axis at a given range ρ using a fast, numerical heuristic known as simulated annealing [47] (SA). A simulated annealing algorithm is employed to solve this optimization problem even though it is not guaranteed to find the global optimum, because it is significantly more computationally efficient than exhaustive search strategies [48, Ch. 3], which

may not be practical in this scenario. The search-area maximization problem is formulated as a nonlinear optimization problem, which are generally considered to be harder than linear problems [49], since solutions can consist of irrational numbers that may not have a finite representation. Simulated annealing time complexity

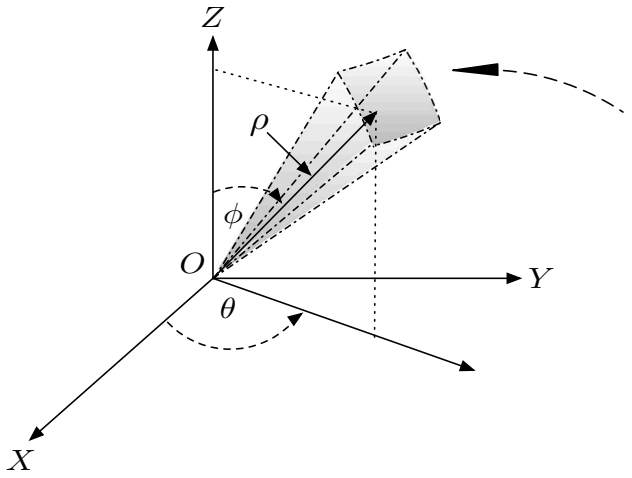

Figure 2.5: A multifunction radar array located at point O searches a sector solid angle Ω with azimuth θ and elevation $\pi - \phi$ at range ρ.

analysis has been primarily studied for maximum matching problems for graphs [50] and convergence results are established in [51],[52].

The inputs to the SA algorithm are the threat axis, search resources, and range. The outputs are the optimal azimuth and elevation angles that maximize the search sector area about the threat axis. The BM and AD search sectors are optimized prior to target launch based on expected BM launch locations and AD threat axes. The AD search sector is then re-optimized after each target-assignment update using the remaining AD search resources. Figs. 2.6(a)-2.6(c) depict the search area optimization results for three different values of T_{search} using a simulated annealing

optimization algorithm.

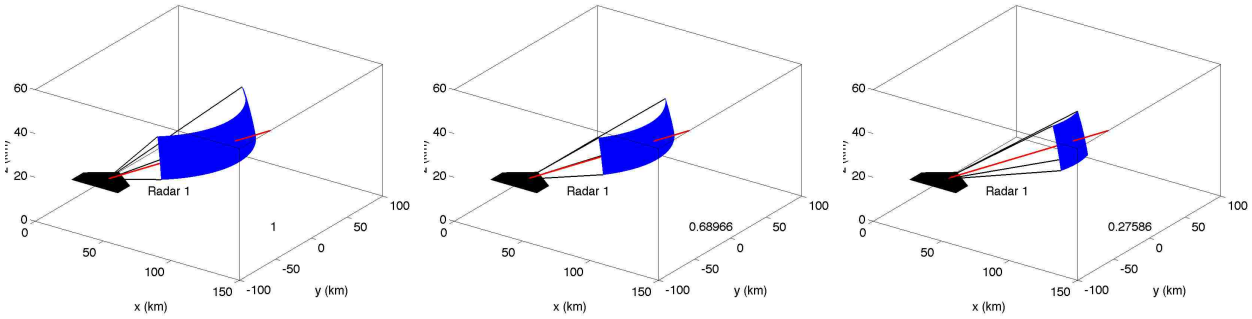

(a) T_{search}=1.0 (b) T_{search}=-0.69 (c) T_{search}=0.28

Figure 2.6: Search area optimization results using simulated annealing for three different normalized values of T_{search}. The search area remains centered on the expected threat axis (denoted by the red line).

2.2.2 Target Kinematics

The kinematics of each ballistic target are modeled as a linear dynamical system after [53],[54, p.61-73], and [55]. Let $X = [x\ y\ z\ \dot{x}\ \dot{y}\ \dot{z}]^T$ be the target state vector (position and velocity) measured by the radar sensor at uniform sampling intervals of time T seconds. Thus $X(n)$ represents the target state at scan n, where the time step is $T = t(n+1) - t(n)$. The acceleration of gravity is g. Let $w(n) \sim \mathcal{N}(0, Q)$ be the Gaussian process noise perturbing the acceleration of the target with zero mean and variance Q. The dynamics of a ballistic target are [53], [56]

$$X(n) = \Phi X(n) + U \begin{bmatrix} 0 \\ 0 \\ -g \end{bmatrix} + w(n), \tag{2.11}$$

where

$$\Phi = \begin{bmatrix} 1 & 0 & 0 & T & 0 & 0 \\ 0 & 1 & 0 & 0 & T & 0 \\ 0 & 0 & 1 & 0 & 0 & T \\ 0 & 0 & 0 & 1 & 0 & 0 \\ 0 & 0 & 0 & 0 & T & 0 \\ 0 & 0 & 0 & 0 & 0 & T \end{bmatrix} \text{ and } U = \begin{bmatrix} T^2/2 & 0 & 0 & T & 0 & 0 \\ 0 & T^2/2 & 0 & 0 & T & 0 \\ 0 & 0 & T^2/2 & 0 & 0 & T \end{bmatrix}^T . \quad (2.12)$$

The measurements collected by a radar at the uniform time intervals T are the range ρ, the azimuth θ, and elevation ϕ, subject to measurement noise with variance $\sigma_\rho^2, \sigma_\theta^2$, and σ_ϕ^2, respectively. Let (x_k, y_k, z_k) be the location of radar k. The relationships between the radar measurements and the target state are [57, pp. 46],[58, pp. 54]

$$\begin{aligned} \rho &= [(x - x_k)^2 + (y - y_k)^2 + (z - z_k)^2]^{1/2} \\ \theta &= \arctan\left(\frac{x - x_k}{y - y_k}\right) \\ \phi &= \arcsin\left(\frac{z - z_k}{\rho}\right). \end{aligned} \quad (2.13)$$

The (nonlinear) measurement equation is

$$Z(n) = h(X(n)) + v(n), \quad (2.14)$$

where $Z = [\rho\ \theta\ \phi]^T$ and $v \sim \mathcal{N}(0, S)$ is the zero mean uncoupled measurement error

with diagonal covariance matrix $S \in \mathbb{R}^{3\times 3}$ referred to in spherical coordinates.

The measurements in 2.14 are transformed to Cartesian coordinates so that the measurement equation is linear (the unbiased and consistent conversion of target measurements to Cartesian coordinates is described in [59]). Let $V \sim \mathcal{N}(0, R)$ be the measurement error with covariance R referred to in Cartesian coordinates as

$$R = \begin{bmatrix} \sigma_x^2 & \sigma_{xy} & \sigma_{xz} \\ \sigma_{xy} & \sigma_y^2 & \sigma_{yz} \\ \sigma_{xz} & \sigma_{yz} & \sigma_z^2 \end{bmatrix}. \tag{2.15}$$

The elements of 2.15 depend on $\sigma_\rho, \sigma_\theta$, and σ_ϕ given by [53]

$$\begin{aligned}
\sigma_x^2 &= \cos^2\theta(\sigma_\rho^2\cos^2\phi + \rho^2\sigma_\phi^2\sin^2\phi) + \rho^2\sigma_\theta^2\sin^2\theta\cos^2\phi \\
\sigma_y^2 &= \sin^2\theta(\sigma_\rho^2\cos^2\phi + \rho^2\sigma_\phi^2\sin^2\phi) + \rho^2\sigma_\theta^2\cos^2\theta\cos^2\phi \\
\sigma_z^2 &= \sigma_\rho^2\sin^2\phi + \rho^2\sigma_\phi^2\cos^2\phi \\
\sigma_{xy} &= \frac{1}{2}\sin 2\theta[(\sigma_\rho^2 - \rho^2\sigma_\theta^2)\cos^2\phi + \rho^2\sigma^2\phi\sin^2\phi] \\
\sigma_{xz} &= \frac{1}{2}\cos\theta\sin 2\phi(\sigma_\rho^2 - \rho^2\sigma_\phi^2) \\
\sigma_{yz} &= \frac{1}{2}\sin\theta\sin 2\phi(\sigma_\rho^2 - \rho^2\sigma_\phi^2).
\end{aligned} \tag{2.16}$$

Finally, the linear measurement equation is

$$Z(n) = H(n)X(n) + V(n), \tag{2.17}$$

where $Z = [x\ y\ z]^T$ and

$$H = \begin{bmatrix} 1 & 0 & 0 & 0 & 0 & 0 \\ 0 & 1 & 0 & 0 & 0 & 0 \\ 0 & 0 & 1 & 0 & 0 & 0 \end{bmatrix}. \tag{2.18}$$

Because 2.11 and 2.17 are both linear with $w(n)$ and $V(n)$ additive white noise Gaussian processes, a Kalman filter provides the optimal (in the minimum mean-squared sense) unbiased estimate of the target state vector.

2.2.3 Radar Track Function

Once a target is detected and track initiation completed, the radar array beam is steered directly to the target [4],[38] for track updates, thus

$$\text{SNR} = \frac{P_t G^2 \lambda^2 \sigma T_{track}}{(4\pi)^3 \kappa T_0 L_s \rho^4}, \tag{2.19}$$

where P_t is the peak transmitter power, G is the antenna gain, λ is the wavelength, and T_{track} is the amount of time the target is in track. Solving for T_{track} we have

$$T_{track} = c\rho^4, \tag{2.20}$$

where

$$c \triangleq (4\pi)^3 \kappa T_0 (SNR) L_s / (P_t G^2 \lambda^2 \sigma). \tag{2.21}$$

Let M_k be the number of targets tracked by radar k so that the total target track time for radar k can be expressed as

$$T_{track,k}^{(tot)} = c \sum_{m=1}^{M_k} \rho_{m,k}^4 \tag{2.22}$$

where $m = \{1, ..., M_k\}$ is the target index.

2.2.4 Target Uncertainty Estimation

A measure of track uncertainty is required by many weapon systems to assess the performance of the target tracking system as well as aid in sensor resource allocation decisions to satisfy the demands of engagement [36],[43],[58, pp. 168]. Fig. 2.7 illustrates how target uncertainty grows over time in the absence of measurements. Successive measurement updates can reduce the target state uncertainty to meet an engagement performance requirement, provided the target update rate is sufficient. In [36] and [60], sensors compute their contribution to a target state estimate based on the reduction in estimate uncertainty. Motivated by this work, the projected reduction in target uncertainty for each radar-target pairing is found based upon the outputs of a minimum variance linear tracking filter. This value is then used to approximate the radar resource requirement (number of measurement updates) to reduce the target uncertainty to a specified level to support an engagement.

Suppose radar j is tracking target m at time step n. Let $x_m(n)$ represent the target state estimate and $\Sigma_m^j(n)$ be the 6×6 error covariance. For each radar k that can track target m, let $\Sigma_m^k(n+1)$ represent the 6×6 error covariance matrix that

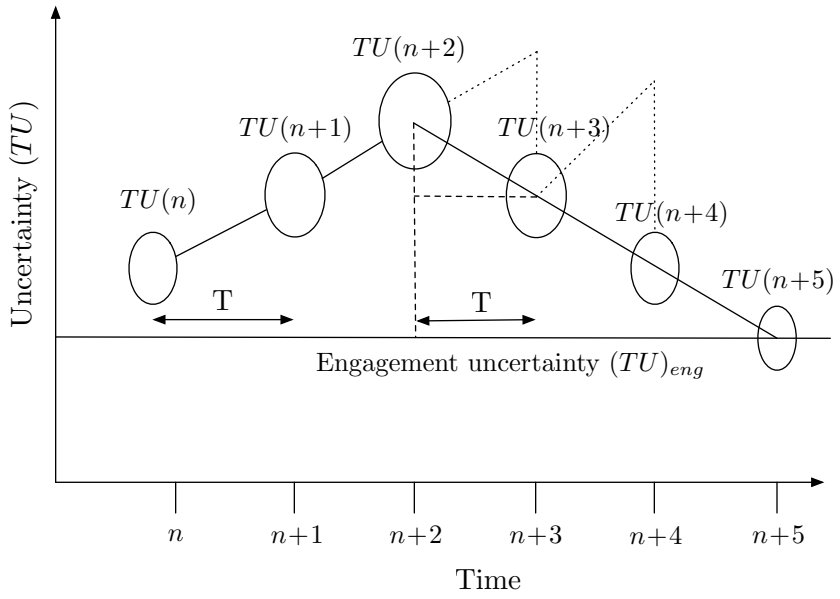

Figure 2.7: Uncertainty growth (no measurements) and reduction (with measurements). The number of measurements required to reduce track uncertainty to the engagement requirement is approximated based on the rate of uncertainty reduction.

would result if, at the next time step, tracking responsibilities for target m switched to radar k. To account for the communication latency between radar j and radar k, the error covariance matrix is expressed as

$$\Sigma_m^k(n) = \begin{cases} \Sigma_m^j(n) & \text{if } k = j \\ \left(\Phi(T_{com})\right)^T \Sigma_m^j(n) \left(\Phi(T_{com})\right) & \text{otherwise,} \end{cases} \tag{2.23}$$

where Φ is the state transition matrix given by 2.12 and T_{com} is the communication latency. Note that 2.23 does not include the process noise covariance, which is assumed identical for all BM targets, and thus would equally scale the track uncertainty values for all radars. (In the case of a non-homogenous BM target environment, the contribution of the process noise covariance to the overall track uncertainty

can be accounted for by adding an additional term $(\Phi(T_{com}))^T Q_m^j(n)(\Phi(T_{com}))$ to 2.23.)

The projected estimate of the Kalman gain at time step $n+1$ if radar k were assigned tracking responsibilities for target m is

$$K_m^k(n+1) = \Sigma_m^k(n)H^T\left[H\Sigma_m^k(n)H^T + R_m^k(n+1)\right]^{-1}, \tag{2.24}$$

where the measurement error covariance R_m^k depends on the position of target m relative to radar k as given in 2.15. The projected state covariance matrix for radar k and target m at time step $n+1$ is then

$$\Sigma_m^k(n+1) = \left(I - K_m^k(n+1)H\right)\Sigma_m^k(n), \tag{2.25}$$

where I is the 6×6 identity matrix. The track uncertainty for each radar-to-target pairing is computed by summing the diagonal position elements of the covariance matrix in 2.25 to obtain

$$(TU)_m^k(n) = \mathrm{Tr}[\Phi^T\Sigma_m^k(n)\Phi]. \tag{2.26}$$

(The appearance of Φ in 2.26 ensures the units of TU are km^2.) Fig. 2.8(a) plots the trajectory of a single BM target that is launched from the origin and the locations of four radars. Fig. 2.8(b) depicts the value of the track uncertainty $(TU)_m^k(n+1)$ for each radar $k \in \{1,2,3,4\}$ assuming a communication latency of $T_{com} = 6$ seconds [60]. The track uncertainty varies according to range and azimuth to the

target, so that Radar 4 does not always provide the smallest track uncertainty despite being closest to the target.

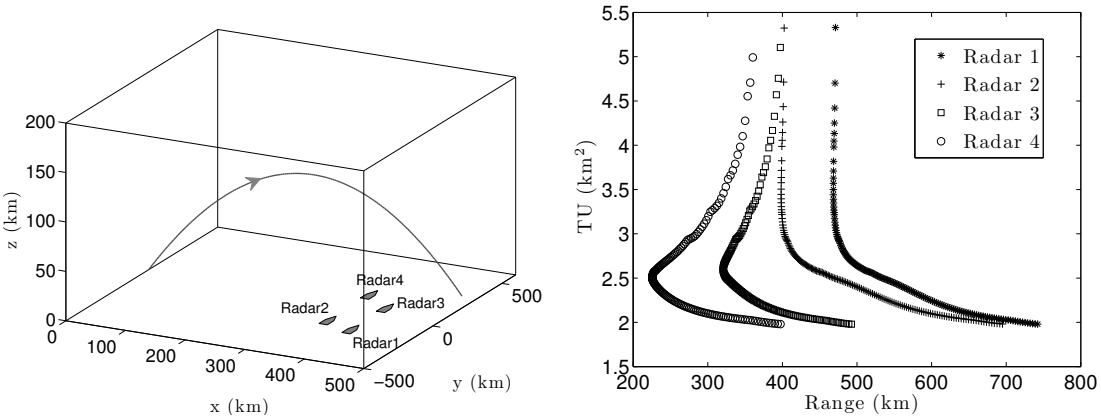

(a) BM trajectory (b) Track Uncertainty

Figure 2.8: (a) Location of $N = 4$ radars relative to a single BM target that launches from (0,0,0); (b) Track uncertainty is not always minimized by the closest radar.

The engagement track uncertainty, $(TU)_{eng}$, may be specified in support of BM and AD engagements; the resources required to reach a desired $(TU)_{eng}$ are computed using a linear interpolation between the current target uncertainty and the projected uncertainty at the next time step. Let $(TU)_m^k(n)$ be the track uncertainty for radar k and target m at time step n using 2.26 with $\Sigma_m^k(n)$ given by 2.25 and let $(TU)_m^k(n+1)$ be the projected track uncertainty for radar k and target m at time step $n+1$. Then the rate of change in track uncertainty between consecutive time steps is

$$\Delta(TU)_m^k = (TU)_m^k(n) - (TU)_m^k(n+1) \tag{2.27}$$

as shown in Fig. 2.2. Let $T_{eng,k}^m$ be the time required for radar k to achieve a desired track uncertainty on target m. Under a linear approximation, the rate of change in

track uncertainty, $\Delta(TU)_m^k$, remains constant so that

$$T_{eng,k}^m = \frac{(TU)_m^k(n) - (TU)_{eng}}{\Delta(TU)_m^k} T_{track,k} = \frac{(TU)_m^k(n) - (TU)_{eng}}{(TU)_m^k(n) - (TU)_m^k(n+1)} T_{track,k}. \quad (2.28)$$

Let M_k be the total number of targets that may be tracked by radar k so that the total target engagement time is

$$T_{eng,k}^{(tot)} = c \sum_{m=1}^{M_k} T_{eng,k}^m. \quad (2.29)$$

Combining 2.9, 2.20, and 2.29 yields the total resources in units of time required to complete the desired search and track functions of radar k and to meet the engagement requirements of all M_k targets. The total resource usage must satisfy

$$T_{search,k}^{(tot)} + T_{track,k}^{(tot)} + T_{eng,k}^{(tot)} + \epsilon_k \leq T_{max}, \quad (2.30)$$

where ϵ_k represents the sum of the resources assigned to other functions and spare resources [3] and T_{max} is the maximum resource availability for each radar. In what follows, $P_k \triangleq (T_{search,k}^{(tot)} + T_{track,k}^{(tot)} + T_{eng,k}^{(tot)} + \epsilon_k)/T_{max}$ denotes the total normalized resources used for search and track by radar k. The radar duty cycle determines the fraction of each transmission cycle that the radar transmitter is active, thus only a fraction of the total radar cycle time may be dedicated to actively searching for or tracking targets. The resource usage constraint is

$$P_k \leq 1, \quad (2.31)$$

which ensures that the combined search, track, and engage resource allocation of each radar will always be less than or equal to unity.

2.3 Interaction Networks and Consensus Behavior

2.3.1 Graph Theory

Communication among coordinated radars is modeled here using graph theory [61], [62] to describe the underlying communication network. A graph $G = (\mathcal{N}, \mathcal{E})$ consists of a set of nodes $\mathcal{N} = \{1, ..., N\}$ and a set of edges $\mathcal{E} \subseteq \mathcal{N} \times \mathcal{N}$ [9]. The edge set $\mathcal{E}$ contains all of the ordered (unweighted) pairs of directed communication links between nodes designated by $e_{jk} \triangleq (j, k)$. If a communication link exists from node j to node k, then node k receives information from node j. An edge is bidirectional when $e_{jk} \in \mathcal{E}$ if and only if $e_{kj} \in \mathcal{E}$. If all of the edges in G are bidirectional, then G is undirected; otherwise G is directed. In a directed graph (digraph), a node k is reachable from node j if there exists a path from j to k that respects the direction of the edges. A digraph is strongly connected if every node is reachable from every other node [61]. The entries a_{kj} in the binary $N \times N$ adjacency matrix A of a graph G with no self-loops are defined as $a_{kj} = 1$ if $e_{jk} \in \mathcal{E}$ and $a_{kj} = 0$ if $k = j$. The Laplacian matrix L of graph G is defined by entries $l_{kj} = -a_{kj}$ for $k \neq j$ and $l_{kk} = \sum_{l=1}^{N} a_{kj}$ [9]. A node j of a digraph G is balanced if the number of edges that originate at node j is equal to the number of edges that terminate at node j (i.e., $\sum_k a_{kj} = \sum_k a_{jk}$). A digraph is called balanced if all of its nodes are balanced.

2.3.2 Radar Communication

The radar communication network is modeled as a strongly connected, balanced digraph G_{com} with nodes $\mathcal{N} = \{1, ..., N\}$ and edges $\mathcal{E}_{com} \subseteq \mathcal{N} \times \mathcal{N}$. The reason for these assumptions is to satisfy the network communication requirements in the target-assignment optimization approach and the binary average-consensus algorithm in Chapter 4. Fig. 2.9(a) illustrates an example of a strongly-connected and balanced directed communication network G_{com} for $N = 4$ radars. If $e_{jk} \in \mathcal{E}_{com}$, then radar j can track targets in radar k's search sector. For each detected target, the target position, velocity, and covariance is exchanged over G_{com}. Each radar k may also broadcast an estimate of their total search resource usage $T^{(tot)}_{search,k}$ over G_{com}, however this is not guaranteed to occur. For the radar communication network G_{com} illustrated in Fig. 2.9(a), the graph Laplacian L_{com} is

$$L_{com} = \begin{bmatrix} 1 & -1 & 0 & 0 \\ 0 & 2 & -1 & -1 \\ -1 & -1 & 2 & 0 \\ 0 & 0 & -1 & 1 \end{bmatrix}. \tag{2.32}$$

2.3.3 Target-Assignment Representation

Graph theory is also used to model the target-assignment network. The target-assignment network $G_{track} = (\mathcal{N} \cup \mathcal{M}, \mathcal{E}_{track})$ is a bipartite graph where

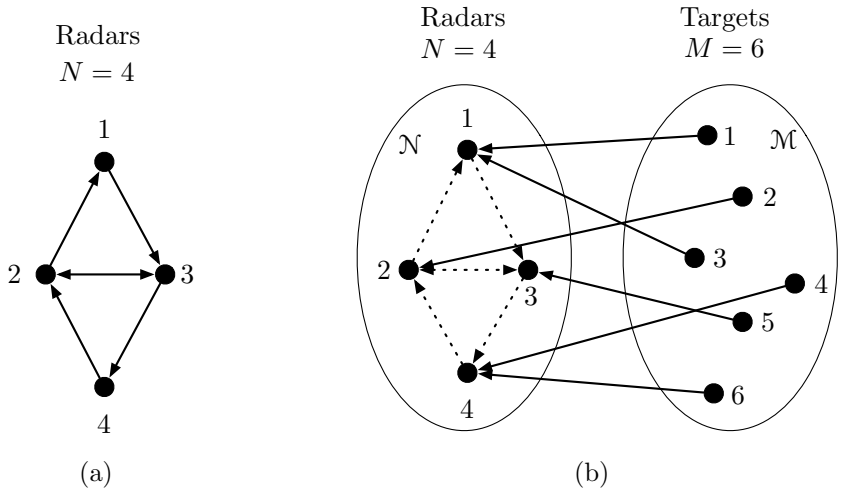

Figure 2.9: Graph-based network models: (a) Radar communication network G_{com} for $N = 4$ radars and (b) target assignment network G_{track} for $M = 6$ targets.

$\mathcal{N} = \{1, ..., N\}$ represents the set of radars, $\mathcal{M} = \{1, ..., M\}$ represents the set of targets, and $\mathcal{E}_{track} \subseteq \mathcal{M} \times \mathcal{N}$ is the unweighted set of all possible radar-to-target pairings. (A bipartite graph is a graph whose vertices can be decomposed into two disjoint sets such that every edge connects a vertex in one set to one in the other set [63],[64].) In the target-assignment problem, each target is tracked by only one radar, however radars can track more than one target. Each (unweighted) edge in the target-assignment graph represents a target-assignment solution that reflects the priorities of resource balancing and resource minimization. Fig. 2.9(b) illustrates one possible target-assignment solution G_{track} for $M = 6$ targets and G_{com} from Fig. 2.9(a).

The optimal target assignment is solved by each radar using a multi-objective optimization approach and then a binary average consensus algorithm is implemented to reach agreement on the global target-assignment. In multiagent networks, consensus means to reach an agreement on a state variable [9], which in this case is

the binary matrix of radar-to-target assignments. A consensus algorithm specifies the interactions and information exchanges between each radar and all of its neighbors on a network [9]. By using a theoretically justified consensus algorithm [9], the initial target-assignment solution identified by each radar will be updated in such a way so as to reach an agreement on a single solution. Consensus algorithms are guaranteed to converge even under very mild assumptions on the communication network [10]; indeed, they are tolerant to time-varying, directed communication links [11] and time-delayed communication [12]. Information can be exchanged either synchronously (radars communicate at the same time using a global clock) or asynchronously (radars take turns communicating without the global clock requirement). An agreement problem in which the agents reach agreement on the average value of their initial states is called an average-consensus problem [65]. Let $x(n) \in \mathbb{R}^N$ represent the states of N nodes at time step n, where $\mathcal{N} = \{1, ..., N\}$, and supposed each node evolves according to the discrete-time [9] dynamics (with step-size $T > 0$)

$$x_k(n+1) = x_k(n) + Tu_k. \tag{2.33}$$

Let $\mathcal{N}_k$ represent the set of all nodes j in the neighborhood of node k (i.e., each node j sends its state information to node k). Olfati-Saber and Murray show [9] that the linear consensus protocol $u_k = \sum_{j \in \mathcal{N}_k}(x_j - x_k)$ solves the average Euclidean consensus problem for agents communicating over a balanced and strongly connected digraph. The dynamics of all nodes can be expressed in terms of the graph Laplacian

L [9]. Let $\epsilon \in (0, 1/\max_k l_{kk})$ where $k \in \{1, ..., N\}$. Then

$$x(n+1) = (I - \epsilon L)x(n). \tag{2.34}$$

Cai and Ishii [65] have extended the average-consensus convergence results in 2.34 to consider strongly connected digraphs that are not balanced and present [66] an average-consensus approach for quantized (integer-valued) information flow on asynchronous networks.

Chapter 3

Distributed Optimization and Validation in Two Dimensions

This chapter presents a dynamic load balancing approach to resource allocation for optimizing the search and track performance of multiple shipboard radars. A 2D linear radar model is introduced in Section 3.2 that is an idealized version of the 3D nonlinear radar model presented in Section 2.2.1. Using the linear model, Section 3.2.1 provides theoretically justified strategies to maximize the collective search area for up to three radars by solving for each radar's optimal location, search-area radius, and search sector. Section 3.2.2 solves for the optimal target-assignment by balancing the search and track tasking among coordinated radars, increasing the number of trackable targets, and show that the assignment boundaries are hyperbolic. Section 3.3 extends the search area maximization and target-assignment optimization approaches from Sections 3.2.1 and Section 3.2.2 to a nonlinear 2D radar model.

3.1 Optimization Approach

To solve the target-assignment problem, each radar seeks the target-assignment solution for the entire network that balances radar resource usage across the radar network. Radar resource usage depends on the search and track requirements. Balancing the resource utilization among coordinated radars prevents a single radar

from using all of its available resources, unless the other radars are also at their maximum capacity, which is important if a majority of the targets are detected by a subset of sensors. Coordinated radars can track targets in another radar's search area; an uncoordinated radar can only track targets within its own search area.

3.2 Linear Radar Model

Recall in a multifunction radar system that the radar performs two primary tasks, search and track [38]. During search, the radar sends out a focused search beam covering a subset of the search sector and looks for a target. If no target is detected, then the search beam moves to the next location until the entire sector is searched. If a target is detected, the radar tracks it by periodically sampling the projected target location. In a variable resource doctrine, if resources are fully consumed by tracking targets, the radar will suspend searching for new targets until resources are freed from tracking requirements. The operating environment is the set of all possible shipboard radar positions $(x, y) \in \mathbb{R}^2$ and target locations. The distance between radar j and radar k is denoted $\delta_{j,k} = \sqrt{(x_j - x_k)^2 + (y_j - y_k)^2}$.

Assume that radar k performs uniform surveillance tasks that consume radar resources as a linear function of both the search coverage sector Ω_k and detection range ρ_k. The detection range is equal to the radius of the search sector and satisfies the requirements of the maximum unambiguous range 2.2. Tracking tasks consume resources as a linear function of the range $\rho_{m,k}$ to the target and number of targets in track (see Fig. 3.1). A resource reserve ϵ_k is also specified, where $0 \leq \epsilon_k \leq 1$,

which represents the fraction of the total (unit) resource that cannot be used for search or track. Each radar communicates over the radar network G_{com} as described in Section 2.3.2.

For $M \geq 2$ targets, a second network, $G_{track} = (\{\mathcal{M}, N\}, E_t)$, called the target-assignment network is considered as discussed in Section 2.3.3. The target assignment problem is to optimize G_{track} given the radar network G_{com}. (In the case of $M = 1$ target, the target assignment problem is to solve for the optimal radar-to-target assignment.) Linear models for resource consumption for search, $T_{search,k}$ and $T_{track,k}$, by radar $k \in \{1, \ldots, N\}$ are

$$T_{search,k} = \mathrm{a}(\rho_k + \Omega_k) \text{ and} \tag{3.1}$$

$$T_{track,k}^{(tot)} = \mathrm{c} \sum_{m=1}^{M_k} \rho_{m,k}, \tag{3.2}$$

where a, c $\in \mathbb{R}_+$ are radar parameters common to each (identical) radar and each radar searches a single sector. Each radar consumes resources to meet its search requirements, but when radars coordinate on target assignment, only the radar assigned to track the target of interest consumes resources for tracking. Since T_{max} is the maximum resource availability of each radar k, the total resource consumed by radar k is

$$P_k = (T_{search,k} + T_{track,k}^{(tot)} + \epsilon_k)/T_{max}, \tag{3.3}$$

with resource reserve constraint

$$P_k \leq 1. \tag{3.4}$$

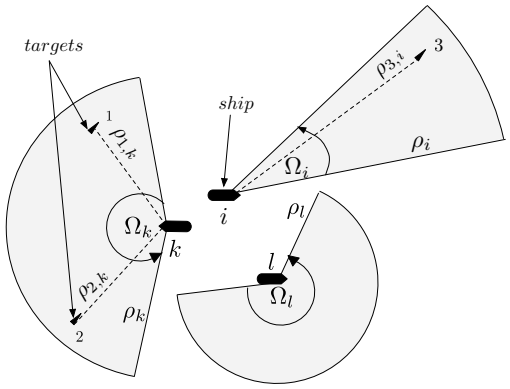

Figure 3.1: Resources for radar k are consumed based on the range $\rho_{m,k}$ to target m and the dimensions (ρ_k, Ω_k) of the search sector in the 2D model.

Equations 3.1–3.4 represent the linearized model of the nonlinear radar range equations 2.7 and 2.20, [4] which determine the resource usage for a multi-function radar. (Note that track uncertainty is not accounted for here.)

3.2.1 Search-Area Maximization

An optimal solution to the search-area problem maximizes the combined search area of N multifunction shipboard radars that can be maintained even after initialization of one or more target tracks. The optimization problem is formulated as follows:

$$\max_x f(x) \text{ s.t. } g(x) \leq 0, \tag{3.5}$$

where x is the collection of variables to be optimized, $f(x)$ is the objective function, and $g(x) \leq 0$ is the constraint. The procedure is described for one-, two-, and three-ship scenarios.

Single-ship Search-Area Maximization

For $N = 1$, $x = \rho$ is the radius of a circular search sector and $f(\rho) = \pi\rho^2$ is the area. $g(\rho)$ represents the resource-use constraint 3.4:

$$\begin{aligned} g(\rho) &= MT(\rho) + S(\rho, 2\pi) + \epsilon - 1 \\ &= \alpha\rho + \beta \leq 0, \end{aligned} \tag{3.6}$$

where

$$\alpha = a + Mc, \text{ and } \beta = 2\pi a - 1 + \epsilon \leq 0. \tag{3.7}$$

The following result is presented for single-ship search area maximization (SAM). The proof of this lemma and all subsequent SAM lemma's are provided in Appendix A.

Lemma 1 (Single-Ship SAM)**.** *Let ρ be the search-sector radius of a single multi-function shipboard radar capable of tracking up to M targets. If $\Omega = 2\pi$, the largest radius ρ^* that can be maintained for the resource reserve ϵ is $\rho^* = -\beta/\alpha$, where α and β are given by 3.7.*

Fig. 3.2(a) illustrates the maximum search area for a single shipboard radar and a single target for three resource reserve values: $\epsilon = 0, 0.3, \text{and } 0.6$; Fig. 3.2(d)

plots the maximum search area as a function of ϵ.

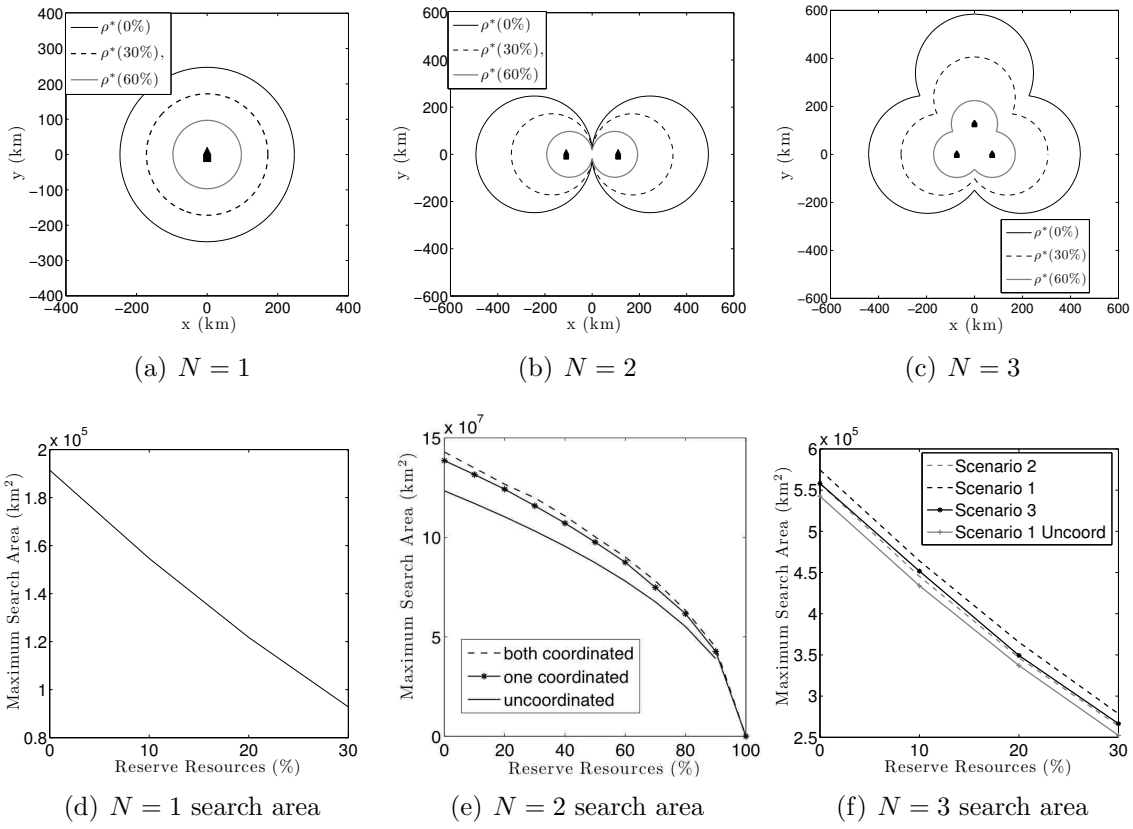

(a) $N = 1$ (b) $N = 2$ (c) $N = 3$

(d) $N = 1$ search area (e) $N = 2$ search area (f) $N = 3$ search area

Figure 3.2: Search-area maximization: The collective search area grows for the same reserve limit with increased radar coordination.

Two Ships Search-Area Maximization

For $N = 2$, $x = (\rho_1, \rho_2, \delta)$ represents the search-area radius ρ_1 of ship $k = 1$, the search-area radius ρ_2 of ship $k = 2$, and the distance $\delta = \delta_{1,2} = \delta_{2,1}$ between the ships. In all cases it is assumed that the resource reserve $\epsilon_1 = \epsilon_2 = \epsilon$. Consider first the case when $\rho_1 = \rho_2 = \rho$ for which $f(\rho_1, \rho_2, \delta_{1,2}) = f(\rho, \delta)$ is the combined search area shown inside the solid lines of Fig. 3.3. (If the search sectors do not overlap, then $\rho_1 = \rho_2 = \rho^*$ as given by Lemma 1.) The total area is calculated by adding

the individual search areas and subtracting the area of overlap. The area of overlap is found by calculating the area of each sector described by $\theta_{1,2} = \theta_{2,1} = \theta$ (use Fig. 3.3 and subtract the area of the triangles 1AB and 2AB). Using the identity $\cos u \sin v = 1/2(\sin(u+v) + \sin(u-v))$, the total area is

$$\begin{aligned} f(\rho, \delta) &= 2\pi\rho^2 - 2\left(\frac{\theta}{2\pi}\pi\rho^2\right) + 4\left(\frac{1}{2}\rho\cos\frac{\theta}{2}\rho\sin\frac{\theta}{2}\right) \\ &= (2\pi - \theta + \sin\theta)\rho^2. \end{aligned} \tag{3.8}$$

An expression for θ in terms of δ and ρ is found by solving $\cos(\theta/2) = \delta/(2\rho)$ for θ. Since $1 - \delta/(2\rho) > 0$ in order for the sensor areas to overlap, this implies that $\delta/(2\rho) < 1$ and therefore $0 < \cos(\theta/2) < 1$, which implies $0 < \theta < \pi$. Note that $\sin\theta - \theta \leq 0$ decreases as $\theta \geq 0$ increases. Thus the total search area is maximized when $\sin\theta - \theta$ is maximized, which corresponds to smaller values of θ. Performing a Taylor series expansion of $\cos(\theta/2)$ about $\theta/2 = 0$ yields

$$\frac{\delta}{2\rho} = \cos\left(\frac{\theta}{2}\right) = 1 - \frac{\theta^2}{8} + \text{H.O.T.} \tag{3.9}$$

The higher order terms in 3.9 are dropped since including them further in the analysis does not significantly affect the values for the overlap angle θ. Solving for θ yields

$$\theta \approx 2\sqrt{2 - \frac{\delta}{\rho}}. \tag{3.10}$$

In the two-ship scenario with overlapping search areas, the area of overlap

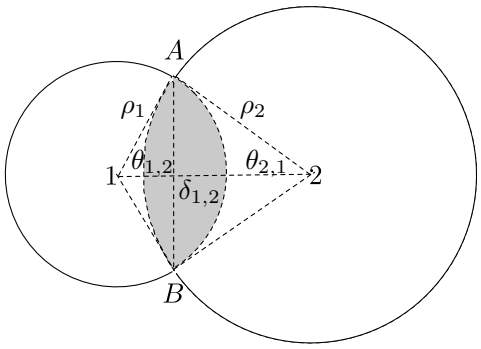

Figure 3.3: Combined search area for two ships.

need not be searched in order to maintain a closed search boundary. The constraint equation 3.4 is

$$\begin{aligned} g(\rho, \delta) &= \alpha\rho + a(2\pi - \theta) + 1 - \epsilon \\ &= \alpha\rho + \beta - a\theta \leq 0, \end{aligned} \tag{3.11}$$

where α and β are given by 3.7.

Lemma 2 (Two Ships SAM - Equal Radii)**.** *Let ρ be the search sector radius of two identical ships separated by $\delta < 2\rho$ and each capable of tracking up to M targets. The maximum search radius ρ^* that can be maintained for the resource reserve ϵ is the largest real root of*

$$b_4\rho^3 + b_3\rho^2 + b_2\rho + b_1 = 0, \tag{3.12}$$

where $b_4 = -5\alpha^3/(6a^3)$, $b_3 = -2\alpha^2\beta/a^3$, $b_2 = -3\alpha\beta^2/(2a^3)$, and $b_1 = 4\pi - \beta^3/(3a^3)$.

The optimal ship separation is

$$\delta^* \approx \rho^* \left(2 - \left(\frac{\alpha\rho^* + \beta}{2a}\right)^2\right). \tag{3.13}$$

Each radar's search radius is solved using 3.12 and position using 3.13. Fig. 3.2(b) illustrates the results of the $N = 2,\ M = 1$ search-area maximization for the same three reserve values.

As shown in Table 3.1, consideration is given to the $N = 2$ case where the optimal search radius of each shipboard radar is sought given their position. Note that the spacing δ must still satisfy $\delta < \rho_1 + \rho_2$.

Lemma 3 (Two Ships SAM - Equal Radii - Given Position)**.** *Given $N = 2$ ships with $\rho_1 = \rho_2 = \rho$ and $\theta_{1,2} = \theta_{2,1}$ that are separated by the distance $\delta_{1,2} = \delta$, the maximum search radius that can be maintained for the resource reserve ϵ is the largest real root of 3.12, where $b_4 = \alpha^2/(4a^2),\ b_3 = 2\alpha\beta/(4a^2), b_2 = \beta^2/(4a^2) - 2$, and $b_1 = \delta$.*

Consider next a scenario in which neither the search radii ρ_1 and ρ_2 nor the overlapping search angles $\theta_{1,2}$ and $\theta_{2,1}$ are equal. One example occurs when $\rho_1 = \rho^*$ (the $N = 1$ optimal radius), and ρ_2 and δ are optimized to maximize the combined search area. This scenario demonstrates the interoperability of the proposed algorithm with pre-existing uncoordinated radar tasking. The objective function $f(\rho_1, \rho_2, \delta)$ is the combined search area and $x = (\rho_1, \rho_2, \delta) = (\rho^*, \rho_2, \delta)$. The combined search area is

$$f(\rho^*, \rho_2, \delta) = \frac{\rho^{*2}}{2}(2\pi - \theta_{1,2} + \sin\theta_{1,2}) + \frac{\rho_2^2}{2}(2\pi - \theta_{2,1} + \sin\theta_{2,1}), \tag{3.14}$$

where

$$\theta_{1,2} = 2\arccos\left(\frac{\delta^2 + \rho^{*2} - \rho_2^2}{2\delta\rho^*}\right) \tag{3.15}$$

and

$$\theta_{2,1} = 2\arccos\left(\frac{\delta^2 - \rho^{*2} + \rho_2^2}{2\delta\rho_2}\right). \tag{3.16}$$

The objective function is maximized when both $\theta_{1,2}$ and $\theta_{2,1}$ are small and the overlap angles are expressed in terms of δ and ρ_2 using Taylor series expansions:

$$\frac{\delta^2 + \rho^{*2} - \rho_2^2}{2\delta\rho^*} \approx \cos\left(\frac{\theta_{1,2}}{2}\right) = 1 - \frac{\theta_{1,2}^2}{8} \tag{3.17}$$

$$\frac{\delta^2 - \rho^{*2} + \rho_2^2}{2\delta\rho_2} \approx \cos\left(\frac{\theta_{2,1}}{2}\right) = 1 - \frac{\theta_{2,1}^2}{8}. \tag{3.18}$$

Solving for $\theta_{1,2}$ and $\theta_{2,1}$ yields

$$\theta_{1,2} \approx 2\sqrt{2\left(1 - \frac{\delta^2 + \rho^{*2} - \rho_2^2}{2\delta\rho^*}\right)} \tag{3.19}$$

$$\theta_{2,1} \approx 2\sqrt{2\left(1 - \frac{\delta^2 - \rho^{*2} + \rho_2^2}{2\delta\rho_2}\right)}. \tag{3.20}$$

The distance δ between the two ships as a function of the search radius ρ_2 and search angle $\theta_{2,1}$ is found by solving 3.20 for δ:

$$\delta^2 + \delta\left(\frac{\rho_2\theta_{2,1}^2}{4} - 2\rho_2\right) + \rho_2^2 - \rho^{*2} \approx 0. \tag{3.21}$$

Table 3.1: Availability of Search-Area Maximization Analytical Results for $N = 2$ and $N = 3$ ships ($\star$ indicates numerical solution, ✓ indicates analytical solution presented in this chapter.)

	Radius given Position			Radius and Position		
	Eq Rad	Two Eq Rad	Uneq Rad	Eq Rad	Two Eq Rad	Uneq Rad
$N = 2$	Lem 3	–	Lem 4	Lem 2	–	✓
Scen 1	Lem 6	Lem 7	Lem 7	Lem 5	✓	✓
Scen 2	Lem 9	$\star$	$\star$	Lem 8	$\star$	$\star$
Scen 3	$\star$	$\star$	$\star$	$\star$	$\star$	$\star$

Solving 3.11 with ρ replaced by ρ_2 and θ replaced by $\theta_{2,1}$ yields

$$\theta_{2,1} = \frac{\alpha\rho_2 + \beta}{b}. \tag{3.22}$$

Substituting 3.22 into 3.21, noting that $\rho_2 \geq \rho^*$, yields two positive real roots with one root less than one and the other greater than one. The larger root is chosen in order to maximize 3.14, which yields

$$\begin{aligned} \delta &= \frac{4}{8a^2}\sqrt{b_6\rho_2^8 + b_5\rho_2^7 + b_4\rho_2^6 + b_3\rho_2^5 + b_2\rho_2^4 + b_1\rho_2^3 + 4a^4\rho^{*2}} \\ &- \frac{1}{8a^2}\left(\alpha^2\rho_2^4 + 2\alpha\beta\rho_2^3 + \beta^2\rho_2^2 - 8a^2\rho_2\right), \end{aligned} \tag{3.23}$$

where $b_6 = \alpha^4/16,\ b_5 = \beta\alpha^3/4,\ b_4 = 3\beta^2\alpha^2,\ b_3 = (\beta^3\alpha/4 - \alpha^2a^2),\ b_2 = (\beta^4/16 - 2\beta\alpha a^2)$, and $b_1 = -\beta^2a^2$.

Using $\sin\theta_{1,2} \approx \theta_{1,2}$ and $\sin\theta_{2,1} \approx \theta_{2,1}$ in 3.14 yields

$$f(\rho^*, \rho_2, \delta) \approx \pi\rho^{*2} - \frac{\theta_{1,2}^3\rho^{*2}}{12} + \pi\rho_2^2 - \frac{\theta_{2,1}^3\rho_2^2}{12}. \tag{3.24}$$

Taking the derivative of 3.24 with respect to ρ_2 gives

$$\frac{\partial f}{\partial \rho_2} = -\frac{1}{4}\rho^{*2}\theta_{1,2}^2\frac{\partial \theta_{1,2}}{\partial \rho_2} + 2\pi\rho_2 - \frac{1}{6}\theta_{2,1}^3\rho_2 - \frac{1}{4}\rho_2^2\theta_{2,1}^2\frac{\partial \theta_{2,1}}{\partial \rho_2}, \tag{3.25}$$

where $\theta_{2,1}$ is given by 3.22 with $\partial\theta_{2,1}/\partial\rho_2 = \alpha/a$, and $\theta_{1,2}$ is given in 3.19. Evaluating $\partial f/\partial\rho_2 = 0$ yields the optimal search radius ρ_2^*, and the results in 3.25 can be used to solve for the optimal spacing δ^*.

The $N = 2$ search area maximization analysis are concluded by considering a scenario in which the search radii ρ_1 and ρ_2 are not equal and the goal is to find the optimal search-sector radius of each ship given their position.

Lemma 4 (Two Ships SAM - Unequal Radii - Given Position)**.** *Given two ships separated by distance $\delta_{1,2} < \rho_1 + \rho_2$, with $\rho_1 = \rho^*$ (the $N = 1$ optimal radius), $\rho_1 \neq \rho_2$, and $\theta_{1,2} \neq \theta_{2,1}$, the maximum search radius $\rho_2{}^*$ that can be maintained for the resource reserve ϵ is the largest real root of*

$$b_4\rho_2^3 + b_3\rho_2^2 + b_2\rho_2^2 + b_1 = 0, \tag{3.26}$$

where $b_4 = \delta\alpha^2/(4a^2)$, $b_3 = 2\delta\alpha\beta/(4a^2) + 1$, $b_2 = \delta\beta^2/(4a^2) - 2\delta$, and $b_1 = \delta^2 + \rho^{*2}$.

Fig. 3.2(e) compares the $N = 2$ maximum search areas for the following three scenarios: (1) both ships coordinating on the combined search area and $\rho_1 = \rho_2 = \rho^*$ from Lemma 2; (2) ship $k = 2$ coordinating on the combined search area and ship $k = 1$ searching with a radius $\rho_1 = \rho^*$ from Lemma 1; and (3) neither ship coordinating on the combined search area, i.e., $\rho_1 = \rho_2 = \rho^*$ from Lemma 1 and δ is

chosen such that $\delta < 2\rho^*$. Note that the combined search area is greater when both ships coordinate the optimization of their search radii and spacing.

Three or More Ships Search-Area Maximization

Consider three or more shipboard multifunction radars that are tasked to protect a prioritized list of defended assets and/or search specific launch areas for targets. Because it is unlikely for $N > 3$ shipboard radars to have overlapping search areas due to the large spacing between the target launch locations as compared to the radar search area, solving the $N = 1,\ 2,$ and 3 search-area maximization problems suggests a solution for an arbitrary number of ships. The $N = 3$ analysis seeks to maximize the combined search area $f(x)$, subject to the reserve constraint $g(x)$, where $x = (\rho_1, \rho_2, \rho_3, \delta_{1,2}, \delta_{1,3}, \delta_{2,3})$ and $\epsilon_1 = \epsilon_2 = \epsilon_3 = \epsilon$. Note $f(x)$ is the total area searched by all three radars less any overlap between radars.

Three possible scenarios are considered for $N = 3$ shipboard multifunction radars, depending on the desired search mission (see Fig. 3.4). Scenario 1 occurs when a single ship's search area overlaps two other ship's search areas but the other two ships do not overlap with each other. Scenario 2 occurs when all three ships have a pairwise search-area overlap with each other but no common overlap area for all three ships. Scenario 3 occurs when all three ships have a common search overlap area. In this scenario, the area of common overlap is called a circular triangle [67].

The combined search area for any of the three $N = 3$ scenarios is calculated by adding the individual search areas and subtracting the total area of overlap. The

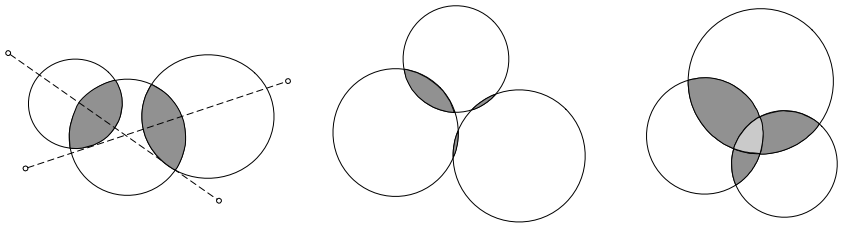

Figure 3.4: Three considered scenarios for $N = 3$ ships.

total area of overlap is found by summing the individual overlap areas of each radar sensor pair as in the $N = 2$ case, where a radar sensor pair is defined as two radars that have a common search area. For Scenario 3, when there exists an overlap area common to all three radars, this area must be added twice to account for the three radar pair overlap area subtractions. The total search area for Scenario $s \in \{1, ..., 3\}$ is

$$f(\rho_1, \rho_2, \rho_3, \delta_{1,2}, \delta_{1,3}, \delta_{2,3}) = \sum_{i=1}^{3} \rho_i^2 \left(\pi + \sum_{j=1, j\neq i}^{3} \frac{\sin \theta_{i,j} - \theta_{i,j}}{2} \right) + V_s \tag{3.27}$$

where $\theta_{i,j}$ is as shown in Fig. 3.3. For Scenario 3, V_4 is the area of the circular triangle [67]; $V_s = 0$ for s = 1,2,3. The following results provide the analytical solutions to Scenarios 1 and 2. Table 3.1 shows a complete listing of the available analytical results for $N = 2$ and $N = 3$ ships.

Lemma 5 (Scenario 1 SAM - Equal Radii)**.** *Let $N = 3$ ships be positioned as in Scenario 1 such that $x_1 < x_2 < x_3$ for all $k = 1, 2, 3$ and $\delta_{1,2} = \delta_{2,3} = \delta$. Let $\rho_1 = \rho_2 = \rho_3 = \rho$. The maximum search radius ρ^* that can be maintained*

for the resource reserve ϵ is the largest root of 3.12, where $b_4 = -5\alpha^3/(3a^3)$, $b_3 = -4\alpha^2\beta/a^3$, $b_2 = (-3\alpha\beta^2)/a^3$, and $b_1 = 6\pi - 2\beta^3/(3a^3)$. The optimal ship separation δ^* is given by 3.13.

Lemma 6 (Scenario 1 SAM - Equal Radii - Given Position)**.** *Let $N = 3$ ships in Scenario 1 be positioned as in Lemma 5 with $\rho_1 = \rho_2 = \rho_3 = \rho$ and $\delta_{1,2} = \delta_{2,3} = \delta$. The maximum radar search radius ρ^* that can be maintained for the resource reserve ϵ is the largest real root of 3.12, where $b_4 = \alpha^2/(4a^2)$, $b_3 = 2\alpha\beta/(4a^2), b_2 = \beta^2/(4a^2) - 2$, and $b_1 = \delta$.*

To satisfy the optimality condition $g(\rho^*, \delta) = 0$, each ship position must satisfy 3.13 for at least one real root ρ^*. Choosing $\delta \leq 2\rho_1$ where ρ_1 is the optimal radius ρ^* from $N = 1$ ensures a solution to 3.13.

Lemma 7 (Scenario 1 SAM - Unequal Radii)**.** *Let $N = 3$ ships in Scenario 1 be positioned as in Lemma 5 with at least two radars having unequal radii and the radius ρ_2 is prescribed. The maximum search radii ρ_1 and ρ_3 are both equal to the largest real root of 3.26.*

Consider next Scenario 1 with $N = 3$ ships positioned as in Lemma 5 with at least two radars having unequal radii. Let $\rho_2 = \rho^*$ from Lemma 1 and $\delta_{1,2} = \delta_{2,3} = \delta$. The objective function $f(\rho_1, \rho_2, \rho_3, \delta)$ is the combined search area and $x = (\rho_1, \rho_2, \rho_3, \delta) = (\rho_1, \rho^*, \rho_3, \delta)$. The combined search area is given in 3.27 with $\theta_{1,2}, \theta_{2,1}, \theta_{2,3},$ and $\theta_{3,2}$ given in A.11–A.14 respectively. The combined search area is maximized when the overlap angle for each ship pair, $\theta_{j,k}$, is small, thus a Taylor series expansion of $\sin\theta_{j,k}$ is performed about $\theta_{j,k} = 0$ in 3.27 to obtain A.16. (In

what follows, the procedure for solving for search radii ρ_1 and ρ_3 are identical, thus only ρ_1 is described.)

The distance $\delta_{1,2}$ as a function of the search radius ρ_1 and search angle $\theta_{1,2}$ is found by solving 3.19 for δ to yield

$$\delta^2 + \delta\left(\frac{\rho^{*2}\theta_{1,2}^2}{4} - 2\rho^*\right) + \rho^{*2} - {\rho_1}^2 \approx 0. \tag{3.28}$$

Solving 3.11 with ρ replaced by ρ_1 and θ replaced by $\theta_{1,2}$ yields

$$\theta_{1,2} = \frac{\alpha\rho_1 + \beta}{b} \tag{3.29}$$

Substituting 3.29 into 3.28, noting that $\rho_1 \geq \rho^*$, yields two positive real roots with one root less than one and the other greater than one. The larger root is chosen in order to maximize 3.27, which yields 3.23 with ρ_2 replaced by ρ_1. Taking the derivative of A.16 with respect to ρ_1 gives

$$\frac{\partial f}{\partial \rho_1} = 2\pi\rho_1 - \frac{1}{6}\theta_{1,2}^3\rho_1 - \frac{1}{4}{\rho_1}^2\theta_{1,2}^2\frac{\partial\theta_{1,2}}{\partial\rho_1} - \frac{1}{4}\rho^{*2}\theta_{2,1}^2\frac{\partial\theta_{2,1}}{\partial\rho_1}, \tag{3.30}$$

where $\theta_{1,2}$ is given by 3.22 with $\partial\theta_{1,2}/\partial\rho_1 = \alpha/a$, and $\theta_{2,1}$ is given by A.12. Evaluating $\partial f/\partial\rho_1 = 0$ yields the optimal search radius ρ_1^*, and the results in 3.30 can be used to solve for the optimal spacing δ^*.

Lemma 8 (Scenario 2 SAM - Equal Radii - Given Position)**.** *Let $N = 3$ sensors be positioned as in Scenario 2 such that $x_1 < x_2$, $x_2 < x_3$, $y_1 > y_2$, and $y_2 < y_3$. Let*

$\rho_1 = \rho_2 = \rho_3 = \rho$ and let ship k's position (x_k, y_k) be known and located such that the separation between all adjacent sensors is equal, i.e., $\delta_{1,2} = \delta_{2,3} = \delta_{1,3} = \delta$. The maximum search radius ρ is the largest real root of 3.12, where $b_4 = \alpha^2/(16a^2)$, $b_3 = \alpha\beta/(8a^2), b_2 = \beta^2/(16a^2) - 2$, and $b_1 = \delta$.

Lemma 9 (Scenario 2 SAM - Equal Radii)**.** *Let $N = 3$ ships with equal radar search radii and spacing be position as in Lemma 8 with σ an optimizing parameter and $\delta \leq 2\rho^*$. The maximum search radius, ρ^*, that can be maintained for the resource reserve ϵ is the largest real root of 3.12, where $b_4 = -\alpha^3/(2a^2)$, $b_3 = -\alpha^2\beta/(a^3)$, $b_2 = -9\beta^2/(2a^3)$, and $b_1 = -(\beta^3/a^3 - 6\pi)$; the optimal ship separation is*

$$\delta^* \approx \rho^* \left(2 - \left(\frac{\alpha\rho^* + \beta}{4a}\right)^2\right). \tag{3.31}$$

For the $N = 3$ cases in which a numerical solution was utilized, a simulated annealing probabilistic search algorithm was implemented to find the optimal radii and spacing using 3.27. The Simulated Annealing Search-Area Maximization Algorithm described in Table 3.2 is a probabilistic search algorithm that finds the maximum value of the combined search area for $N = 3$ ships by always accepting better values of the combined search area and accepting worse values with a decreasing probability. The algorithm terminates upon reaching the maximum number of successful tries with the same values of ρ and δ. Fig. 3.2(c) illustrates the optimal solution to Scenario 2 for $N = 3$, when $\rho_1 = \rho_2 = \rho_3 = \rho$ and $\delta_{1,2} = \delta_{2,3} = \delta_{1,3} = \delta$. Fig. 3.2(f) plots the combined search areas versus ϵ for $N = 3$ ships and all three scenarios, and for Scenario 1 when none of the ships coordinate on the combined

Table 3.2: **Simulated Annealing Search-Area Maximization Algorithm** [47]

Input: Perturb function to update the input values X, $h(X) : \mathbb{R}^n \to \mathbb{R}^n$, cost function $J : \mathbb{R}^n \to \mathbb{R}$ to compare candidate solutions, constraint function $G : \mathbb{R}^n \to \mathbb{R}$, and a non-increasing cooling schedule $T(n+1) = kT(n)$,where $0 < k < 1$.

Initialize: Estimate at current time step, $X(1)$.

Complete the following steps for $n = 1, 2, 3...$ until a termination criteria is reached.

1. Generate $X'(n) = h(X(n))$ and calculate $J(X(n))$ and $J(X'(n))$
2. Set $J(X'(n)) = 0$ if $G(X'(n)) > 0$. (constraint violated)
3. Sample from a uniform distribution $r \sim \mathbb{U}(0, 1)$ and update X according to:

$$X(n+1) = \begin{cases} X'(n) & \text{if } r < \exp\left(\frac{-(J(X(n))-J(X'(n)))}{kT(n)}\right) \\ X(n) & \text{otherwise} \end{cases}$$

where $T(n)$ is the current temperature.

4. Update the temperature based on the cooling schedule.

search area.

3.2.2 Target Assignment Optimization

This section poses and solves an optimal target-assignment problem that seeks to balance the search and track tasking between multi-function radar systems. It starts by considering $M = 1$ target for $N = 3$ shipboard multifunction radars and shows that the solution to the target-assignment problem has a hyperbolic boundary determined by the search-area radii and distance to the target. The results are extended to $M > 1$ targets and the target assignment boundary for target M is solved for, assuming targets $1, ..., M-1$ are already being tracked. In each case it is assumed that all $N = 3$ ships have exact knowledge of the position of targets

$1, ..., M$. A combination of analytical and numerical solutions are presented to highlight the results.

Prior knowledge of the hyperbolic "switching" boundary for multi-function radars has many benefits. For example, target handovers or migrations can negatively affect the accuracy of the target state information during the time it takes the new tracking radar to search for and acquire the target, even with accurate information from the previous tracker. Knowledge of the target-switching boundary also allows a radar to be prepared to track a new target, in effect the radar is cued beforehand and can plan tasking accordingly. Another benefit of knowing the target-assignment boundary is the ability to optimize the ship and radar placement relative to the target(s). Finally, in the event that a target is or will be soon engaged, the target-switching boundary allows for radars to anticipate a handover that may occur during or just prior to an engagement order and thus delay or prevent the target from switching from one radar to another avoid any loss or degradation in the target state information.

Four possible cases of radar performance are considered to evaluate the target-assignment algorithm. Case (i) – Unoptimized/Uncoordinated occurs when the radars do not optimize their combined search area and do not coordinate on the target assignment. Case (ii) – Unoptimized/Coordinated occurs when the radars do not optimize their combined search area but coordinate on the target assignment. This case could arise when the radar locations are fixed or when the radar ship platforms must remain in a particular location for other operational mission requirements. Case (iii) – Optimized/Uncoordinated occurs when the combined

search area is optimized but the radars do not coordinate on the target assignment. This case could arise if the ship positions and radar search radii were remotely optimized prior to arriving on station. Case (iv) – Optimized/Coordinated occurs when the combined search area is optimized and the radars coordinate on the target assignment.

Single Target Assignment

Recall the total resource loading P_k of ship k defined in 3.3. A balanced radar resource loading between all pairs of communicating radars can be accomplished by minimizing the absolute value of the difference $|P_k - P_l|$ between their loading for all connected pairs k, l, consistent with the resource reserves $\epsilon_k,\ \epsilon_l$. By minimizing the difference between the total resource loading between each shipboard radar pair, a balanced radar resource loading among all radars is achieved. A balanced approach is shown here to increase the trackable area and allow more targets to be tracked within a given search area.

Let $M = 1$ and j be the index of the tracking ship. The measure of resource balancing among all ships is

$$C_j(G_{com}) = \sum_{(k,l)\in E_s} (P_k - P_l)^2 \,, \tag{3.32}$$

where G_{com} is the (undirected) ship communication network. The optimal target assignment for G_{com} that balances the radar tasking between all pairs of ships is

$$j^* = \underset{j \in \{1,\ldots,N\}}{\operatorname{argmin}} \; C_j(G_{com}). \tag{3.33}$$

The optimal target assignment for $N = 3$ ships and $M = 1$ target is computedusing the target-assignment optimization algorithm in Table 3.3. Note that the set of possible target positions assigned to a ship is called the track zone. Fig. 3.5(a) illustrates the solution to the target-assignment problem for Cases (i)–(iv) introduced earlier. Note that in Case (ii) (three ships whose search area is not optimized but coordinate on target assignment) ship $k = 1$ and ship $k = 3$ are assigned tracking responsibilities inside ship $k = 2$'s search area. Also note that in Case (iii) (three ships whose search area is optimized but are not coordinated on target assignment) all ships track target $M = 1$ in their respective search overlap areas, thus expending twice as many resources as necessary.

Fig. 3.5(b) compares the radar tasking of all four cases and verifies that the optimal target assignment balances radar tasking. In the cases where the search area and ship positions are optimized, the optimal solution also yields an increase in the trackable area.

For Cases (ii) and (iv) (all three ships coordinate their target assignment), the solution to the target assignment problem for any pair of ships is a conic section that describes the boundary between the track zones. In Case (ii) the solution is a pair of hyperbolic boundaries, whereas in Case (iv) the solution is a line.

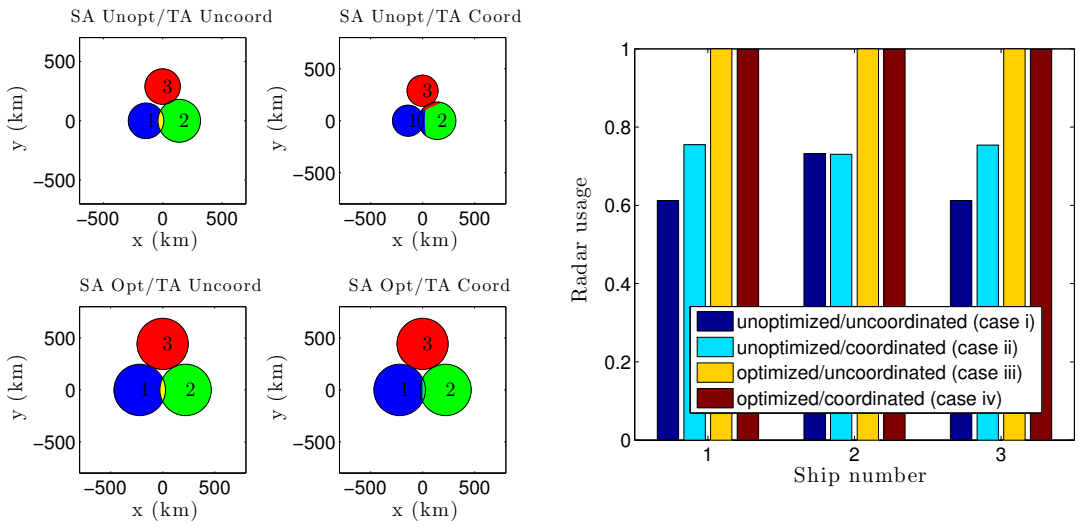

(a) Optimal target assignment

(b) Resource loading

Figure 3.5: Target Assignment for $N = 3$ ships: Coordinated target assignment increases the trackable area and balances radar tasking. Tracking area for a single target for ships 1, 2 and 3 are highlighted in blue, green, and red respectively. Yellow indicates more than one ship assigned to track a single target in this area.

Theorem 1 (Single-Target Assignment)**.** *Let* $(x_j, y_j), (x_k, y_k)$, *and* (x_m, y_m) *be the positions of ship* j, *ship* k, *and target* m *respectively. The solution to the target-assignment problem is a hyperbolic boundary given by the solution to*

$$\sqrt{(x_j - x_m)^2 + (y_j - y_m)^2} - \sqrt{(x_k - x_m)^2 + (y_k - y_m)^2} = \frac{T_{search,k} - T_{search,j}}{c}, \tag{3.34}$$

where $T_{search,j}$ *and* $T_{search,k}$ *are given in 3.1 and* c *is a positive constant given in 3.2.*

Proof. Let P_j and P_k be the radar tasking required by ships j and k to track target $m = M = 1$ as in 3.3. The optimal solution to the target-assignment problem switches from ship j to ship k as the target passes through the boundary defined by

Table 3.3: Single Target Assignment Algorithm

Input: The ship communication network G_{com}, resource reserve ϵ_k, and the position, search radii and sector of each ship radar. At each timestep and for $M = 1$ target:

1: Calculate $T_{search,k}, T_{track,k}$ and P_k according to 3.1, 3.2, and 3.3 for each ship k.

2: Compute C_j, according to 3.32 where $j \in \{1, 2, 3\}$ denotes the tracking ship, and choose j^* according to 3.33.

$P_j = P_k$ or, equivalently,

$$\begin{aligned} T_{search,j} + T_{track,j} &= T_{search,k} + T_{track,k} \\ \rho_{m,j} - \rho_{m,k} &= \frac{T_{search,k} - T_{search,j}}{c}. \end{aligned} \tag{3.35}$$

When $T_{search,j} < T_{search,k}$, then to satisfy the equality condition, $T_{track,j} > T_{track,k}$. From 3.2, this implies $\rho_{m,j} > \rho_{m,k}$ and only one branch of the hyperbolic boundary satisfies 3.35, which completes the proof. □

Corollary 1. *For Case (iv) when $T_{search,j} = T_{track,k}$, this implies $\rho_{m,j} = \rho_{m,k}$. Thus the target boundary is described by*

$$y = -\frac{x_k - x_j}{y_x - y_j}x - \frac{x_j^2 - x_k^2 + y_j^2 - y_k^2}{2(y_j - y_k)}, \tag{3.36}$$

which is the equation of a straight line.

While the previous results provide an analytical solution to the $M = 1$ target assignment boundaries for radars that are both optimized and unoptimized, it is also instructive to compute the track zones for each ship. The track zone $Z_k^{(M)}$ for ship k and target M is defined as the set of all possible target positions inside the

combined search area for ships $j = 1, ..., N$, where ship j coordinates with ship k such that the resource loading is most balanced when ship k tracks target M. The following is a mathematical description of $Z_k^{(M)}$.

Proposition 1 (Single-Target Track Zone)**.** *Let $(x, y) \in \mathbb{R}^2$ be the position of target $M = 1$. The track zone $Z_k^{(M)}$ for ship k is the set $Z_k^{(M)} = \bigcap_{j=1}^{N} Z_{k,j}^{(M)}$, where*

$$\begin{aligned} Z_{k,j}^{(M)} \quad = \quad & \Big\{(x,y) | \sqrt{(x_k - x)^2 + (y_k - y)^2} \leq \rho_k + \rho_{j,k} \bigcap \\ & \sqrt{(x_j - x)^2 + (y_j - y)^2} \leq \rho_j \bigcap \\ & \sqrt{(x_k - x)^2 + (y_k - y)^2} + a\rho_k + b\Omega_k \leq (1 - \epsilon) \bigcap \\ & \sqrt{(x_k - x)^2 + (y_k - y)^2} \leq \sqrt{(x_j - x)^2 + (y_j - y)^2} + \frac{a\rho_j + b\Omega_j - a\rho_k - b\Omega_k}{c} \Big\}. \end{aligned} \tag{3.37}$$

Fig. 3.6 depicts the analytical solution to the target assignment boundaries and track zones for Case (ii) when the radars are unoptimized and coordinated.

Multi-Target Assignment

For $M > 1$ targets, the objective is to balance the radar tasking among all shipboard radars in the communication network G_{com}, where the radar tasking P_k for ship k now includes the total tracking cost for all M_k targets assigned to ship k. The measure of the resource balancing among all ships and all targets for a particular target-assignment network G_{track} and ship communication network G_{com}

is

$$C(G_{track}; G_{com}) = \sum_{(k,l)\in E_s} (P_k(G_{track}) - P_l(G_{track}))^2. \tag{3.38}$$

Let $G^*_{track} = \text{argmin}_{G_{track}} C(G_{track}; G_{com})$ be the optimal target-assignment network that balances the radar tasking across ship network G_{com}. Then G^*_{track} is computed using the multi-target assignment algorithm in Table 3.4. For shipboard radars that coordinate on their target assignment for multiple targets, the following result is presented.

Theorem 2 (Multi-Target Assignment)**.** *For each pair of ships j, k that coordinate on their target assignment, let $m = \{1, ..., M_j\}$ be the indices of targets tracked by ship j and $l = \{1, ..., M_k\}$ be the indices of targets tracked by ship k, where $M_j + M_k = M - 1$. The target assignment boundary for target M is the solution to*

$$\begin{aligned}\sqrt{(x_M - x_j)^2 + (y_M - y_j)^2} - \sqrt{(x_M - x_k)^2 + (y_M - y_k)^2} \;&= \\ \frac{T_{search,k} - T_{search,j}}{c} - \sum_{m=1}^{M_j} \sqrt{(x_m - x_j)^2 + (y_m - y_j)^2} \;&+ \\ \sum_{l=1}^{M_k} \sqrt{(x_l - x_k)^2 + (y_l - y_k)^2}.&\end{aligned} \tag{3.39}$$

Proof. Let $T^{(tot,m)}_{track,j}$ and $T^{(tot,l)}_{track,k}$ be the total resources consumed by ships j and k to track targets m and l. The optimal solution to the target assignment problem for the target M switches from j to k as the target passes through the boundary $P_{j,M} = P_{k,M} - T^{(tot,m)}_{track,j} + T^{(tot,l)}_{track,k}$ or equivalently

$$\rho_{M,j} - \rho_{M,k} = \frac{T_{search,k} - T_{search,j}}{c} - \sum_{m=1}^{M_j} \rho_{m,j} + \sum_{l=1}^{M_k} \rho_{l,k}, \tag{3.40}$$

Table 3.4: Multi-Target Assignment Algorithm

Input: Same as the Single-Target Assignment Algorithm in Table IV.
At each timestep and for each target assignment network $G_{track} = (\mathcal{M}, E_t)$:
1: Calculate $P_k(G_{track})$ according to 3.1, 3.2, and 3.3.
2: Calculate $C(G_{track}; G_{com})$ according to 3.38.
3: Find the target assignment network G^*_{track} that minimizes $C(G_{track}; G_{com})$.

which yields 3.39 and completes the proof. □

Corollary 2. *When* $T_{search,k} = T_{search,j}$, *then* $\rho_{M,k} = \rho_{M,j} + \sum_{m=1}^{M_j} \rho_{m,j} - \sum_{l=1}^{M_k} \rho_{l,k}$. *The target boundary for target* M *is the line found by solving*

$$\begin{aligned} &\sqrt{(x_M - x_k)^2 + (y_M - y_k)^2} \;-\; \sqrt{(x_M - x_j)^2 + (y_M - y_j)^2} \\ &- \sum_{m=1}^{M_j} \sqrt{(x_j - x_m)^2 + (y_j - y_m)^2} \;+\; \sum_{l=1}^{M_k} \sqrt{(x_l - x_k)^2 + (y_l - y_k)^2} = 0. \end{aligned} \tag{3.41}$$

The multi-target track zone $Z_k^{(M)}$ is a function of the positions of the targets already being tracked by ship k and ship j. For ship k and target $M > 1$, $Z_k^{(M)}$is defined as the set of all possible target positions inside the combined search area for ship $j = 1, ..., N$, where ship j coordinates with ship k such that the resource loading is most balanced when ship k tracks target M, assuming M_j is the number of targets already being tracked by ship j. The following is a mathematical description of the multi-target track zone.

Proposition 2. *Let* $(x, y) \in \mathbb{R}^2$ *be the position of target* $M > 1$. *The track zone*

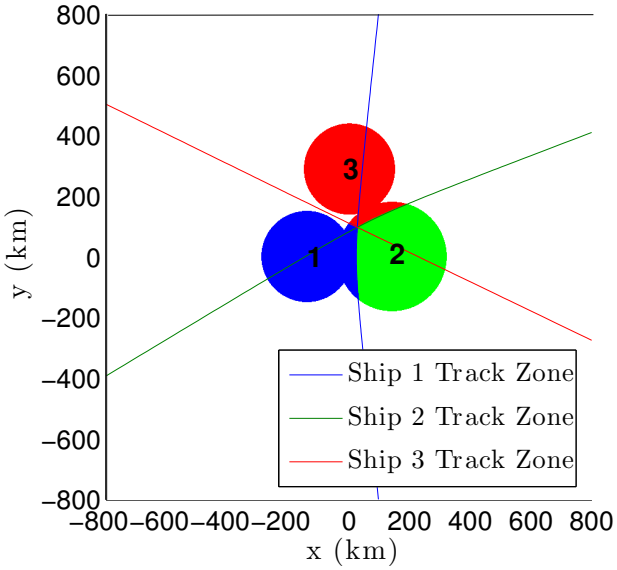

Figure 3.6: Analytical optimal target assignment boundaries and track zones for $M = 1$ target.

$Z_k^{(M)}$ for ship k is the set $Z_k^{(M)} = \bigcap_{j=1}^{\mathrm{N}} Z_{k,j}^{(M)}$, *where*

$$
\begin{aligned}
Z_{k,j}^{(M)} \;=\; & \Big\{(x,y)\,|\,\sqrt{(x_k-x)^2+(y_k-y)^2} \le \rho_k + \rho_{j,k} \bigcap \\
& \sqrt{(x_j-x)^2+(y_j-y)^2} \le \rho_j \bigcap \\
& \sqrt{(x_k-x)^2+(y_k-y)^2} + a\rho_k + b\Omega_k \le (1-\epsilon) \bigcap \\
& \sqrt{(x_k-x)^2+(y_k-y)^2} < \sqrt{(x_j-x)^2+(y_j-y)^2} + \frac{a(\rho_j-\rho_k)+b(\Omega_j-\Omega_k)}{c} \\
- \; & \sum_{m=1}^{M_j} \sqrt{(x_j-x_m)^2+(y_j-y_m)^2} + \sum_{l=1}^{M_k} \sqrt{(x_k-x_l)^2+(y_k-y_l)^2} \Big\}.
\end{aligned}
\tag{3.42}
$$

Figs. 3.7(a)–3.7(c) illustrate how the multi-target assignment boundaries and track zones for the second of two targets changes as the first target passes through the combined search area of three ships. (The target assignment boundaries and

track zones for the first target are shown in Fig. 3.6) The first target is depicted by a black dot. In Fig. 3.7(a), target $M = 1$ is being tracked by the leftmost ship located at (-150,0). In Fig. 3.7(b), target $M = 1$ is still tracked by the same ship, however it is approaching the edge of the $M = 1$ target assignment boundary. In Fig. 3.7(c), the first target has crossed the $M = 1$ target assignment boundary and is now being tracked by the rightmost ship located at (150,0).

3.3 Nonlinear Radar Model

This section presents a Search Area Maximization and Target-Assignment Optimization approach using a 2D nonlinear model for radar search and track resource allocation. The identical $N = 1, 2,$ and 3 ship scenarios from Sections 3.2.1 and 3.2.2 are considered. Due to the similarity of the approach in this section as compared to the previous section, the optimization approach is only briefly reviewed; the majority of this subsection focuses on the optimization results, which reinforce the results of the linear model.

The radar search and track equations given in 3.1 and 3.2 respectively are modified to account for resource consumption as the fourth power of range. Thus

$$T_{search,k} = \mathrm{a}\rho_k^4\Omega_k \quad \text{, and} \tag{3.43}$$

$$T_{track,k}^{(tot)} = \mathrm{c}\sum_{m=1}^{M_k}\rho_{m,k}^4, \tag{3.44}$$

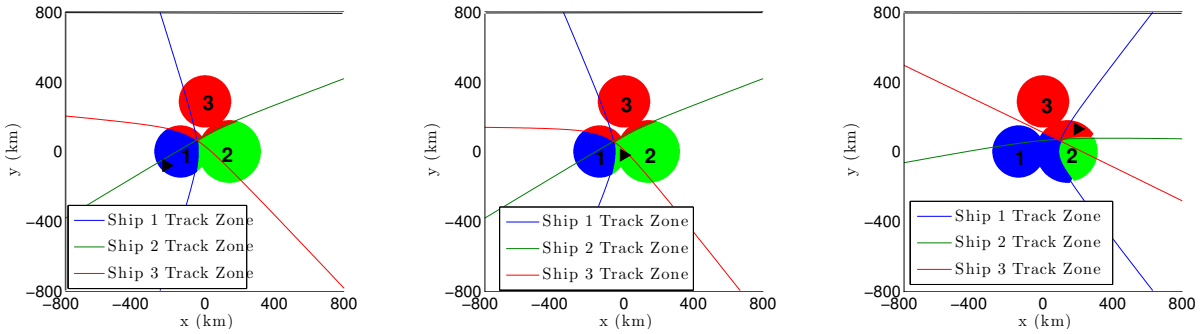

(a) t=60s (b) t=154s (c) t=248s

Figure 3.7: Multi-target assignment boundaries and track zones for the second of two targets, which change as a function of the first target's position (shown as black dot). The target velocity is 2.5 km/sec [68].

where a, c are given by 2.8 and 2.21 respectively, $\rho_k, \Omega_k,$ and $\rho_{m,k}$ are given by 3.1 and 3.2 respectively, and the total normalized resource usage P_k is given by 3.4.

3.3.1 Search-Area Maximization

Single Ship SAM

For $N = 1$, $x = \rho$ is the radius of a circular search sector and $f(\rho) = \pi\rho^2$ is the area. The resource-use constraint $g(\rho)$ is:

$$\begin{aligned} g(\rho) &= MT_{track}(\rho) + T_{search}(\rho, 2\pi) + \epsilon - 1 \\ &= \alpha\rho^4 + \beta \leq 0, \end{aligned} \tag{3.45}$$

where α and β are given by 3.7. Let ρ be the search-sector radius of a single ship capable of tracking up to M targets and let $\Omega = 2\pi$. Since $f(\rho)$ monotonically increases with ρ and $\alpha > 0$, then ρ^* satisfies $g(\rho^*) = 0$ and the largest radius ρ^* that

can be maintained for the resource reserve ϵ is

$$\rho^* = |(-\beta/\alpha)^{\frac{1}{4}}| > 0. \tag{3.46}$$

Fig. 3.8(a) and 3.8(d) plots the $N = 1$ results for $\epsilon = 0, 0.3, 0.6$.

Two- and Three-Ship Search-Area Maximization

The collective search area of $N = 2$ and $N = 3$ ships is maximized using the Simulated Annealing Search-Area Maximization Algorithm in Table 3.2 and the nonlinear resource constraint

$$g(\rho, \delta) = \alpha\rho^4 - a\theta\rho^4 + \beta \leq 0. \tag{3.47}$$

Figs. 3.8(b); 3.8(e), 3.8(c), and 3.8(f) plot the $N = 2$ and $N = 3$ results, respectively. Note that in both cases, the collective search area is larger if at least one ship is able to coordinate on the collective search area.

3.3.2 Target Assignment Optimization

Single Target Assignment

To compute the optimal target assignment for $N = 3$ ships and $M = 1$ target for Cases (i)–(iv) described in Section 3.2.2, the single-target assignment algorithm in Table 3.3 is used. Ship 1 and ship 2 optimize their $N = 2$ collective search-area using Table 3.2, whereas ship 3 optimizes its search area using 3.46. Fig. 3.9(a)

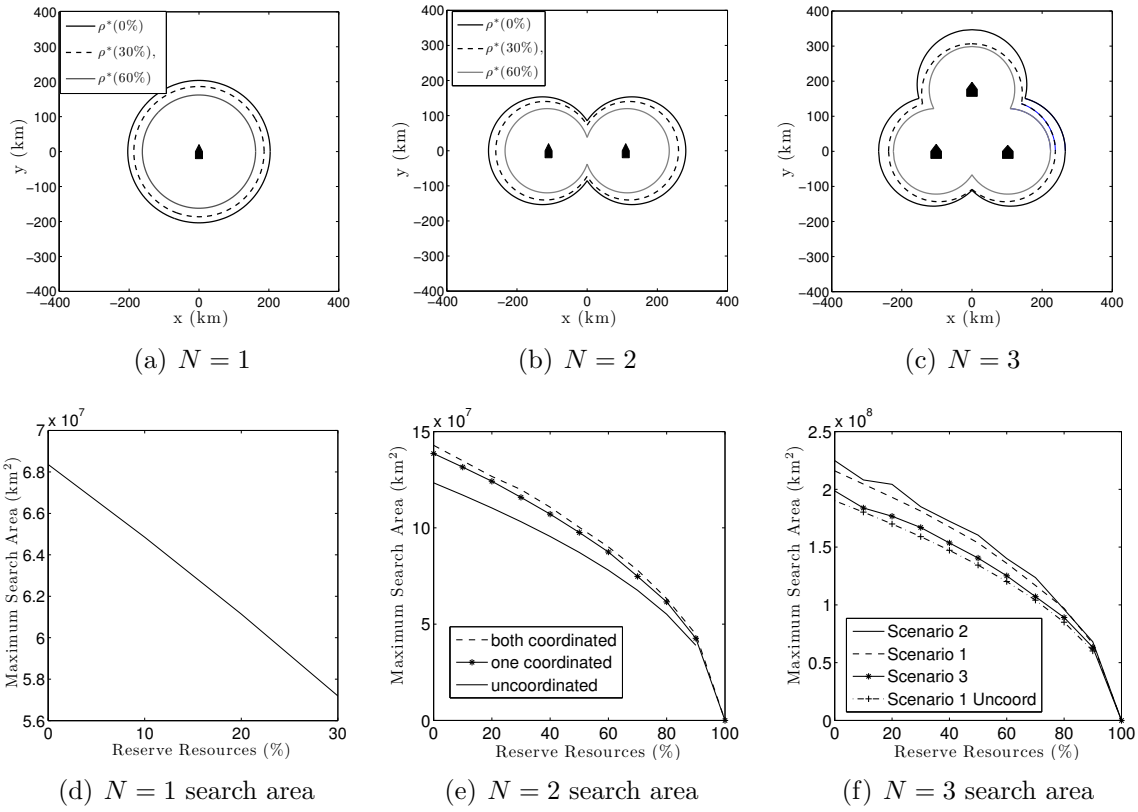

(a) $N = 1$ (b) $N = 2$ (c) $N = 3$

(d) $N = 1$ search area (e) $N = 2$ search area (f) $N = 3$ search area

Figure 3.8: 2D nonlinear search-area maximization: The search area is maximized when at least one shipboard radar is able to coordinate.

illustrates the results. Note that in Case (ii), the track zone for ship 1 extends into the search area of ship 2. Also observe that in both Case (i) and Case (iii) (target-assignment uncoordinated), ships 1 and 2 track target $M = 1$ in their areas of search overlap (highlighted in yellow), thus expending twice as many resources as necessary due to redundant tracking. In Case (iv), ships 1 and 2 partition tracking responsibilities in their collective search area by balancing their resource usage. Fig. 3.9(b) compares the radar tasking of all four cases and verifies that the optimal target assignment balances radar tasking. In Case (iv), the optimal solution also increases the trackable area by reducing the resource loading.

To determine the target-assignment boundary, let P_j and P_k be the radar

tasking required by ships j and k to track target $m = M = 1$ as in (4). The optimal solution to the target-assignment problem switches from ship j to ship k as the target passes through the boundary defined by $P_j = P_k$ or,

$$\left((x_j - x)^2 + (y_j - y)^2\right)^2 - \left((x_k - x)^2 + (y_k - y)^2\right)^2 = \frac{S_k - S_j}{c}. \tag{3.48}$$

Because of the nonlinearity, the boundary is no longer hyperbolic.

For Case (iv) when $S_j = S_k$, this implies ${\delta_{j,m}}^4 = {\delta_{k,m}}^4$. Thus the target boundary 3.48 is the equation of a line given by

$$y = -\frac{x_k - x_j}{y_k - y_j}x - \frac{x_j^2 - x_k^2 + y_j^2 - y_k^2}{2(y_j - y_k)}. \tag{3.49}$$

which is identical to the linear result in 3.36.

Multi-Target Assignment

In the case of $M > 1$ targets, the objective is to balance the radar tasking among all shipboard radars in the communication network G_{com}, where the radar tasking P_k for ship k now includes the total tracking cost for all M_k targets assigned to ship k. The measure of resource balancing is given by 3.38 and $G^*_{track} = \text{argmin}_{G_{track}}\ C(G_{track}; G_{com})$ is the optimal target- assignment network that balances radar tasking across ship network G_{com}. The multi-target assignment algorithm in Table 3.4 is used to compute G^*_{track}.

For each pair of ships j, k that coordinate on their target assignment, let

$m = \{1, ..., M_j\}$ be the indices of targets tracked by ship j and $l = \{1, ..., M_k\}$ be the indices of targets tracked by ship k, where $M_j + M_k = M - 1$. Let $T^{(tot)}_{track,j}$ and $T^{(tot)}_{track,k}$ be the total resources consumed by ships j and k to track targets m and l.

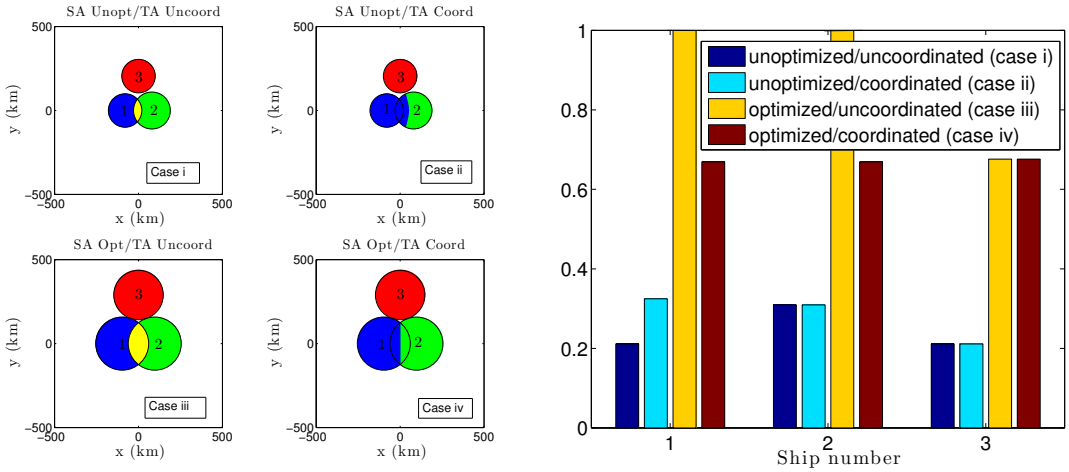

(a) Optimal target assignment

(b) Resource loading

Figure 3.9: Target Assignment for $N = 3$ ships: Coordinated target assignment increases the trackable area and balances radar tasking. Tracking area for a single target for ships 1, 2 and 3 are highlighted in blue, green, and red respectively. Yellow indicates more than one ship tracking in this area.

The optimal solution to the target assignment problem for target M switches from j to k as the target passes through the boundary $P_{j,M} = P_{k,M} - T^{(tot)}_{track,j} + T^{(tot)}_{track,k}$. When $S_k = S_j$, then the target boundary for target M is the line found by solving

$$\begin{aligned} &\left((x_k - x_M)^2 + (y_k - y_M)^2\right)^2 - \left((x_j - x_M)^2 + (y_j - y_M)^2\right)^2 = \\ &\sum_{m=1}^{M_j} \left((x_j - x_m)^2 + (y_j - y_m)^2\right)^2 + \sum_{l=1}^{M_k} \left((x_k - x_l)^2 + (y_k - y_l)^2\right)^2. \end{aligned} \tag{3.50}$$

Figs. 3.10(a)–3.10(c) illustrate how the multi-target assignment boundaries and track zones for case (ii) for the second of two targets changes as the first target passes through the combined search area of three ships. The first target is depicted

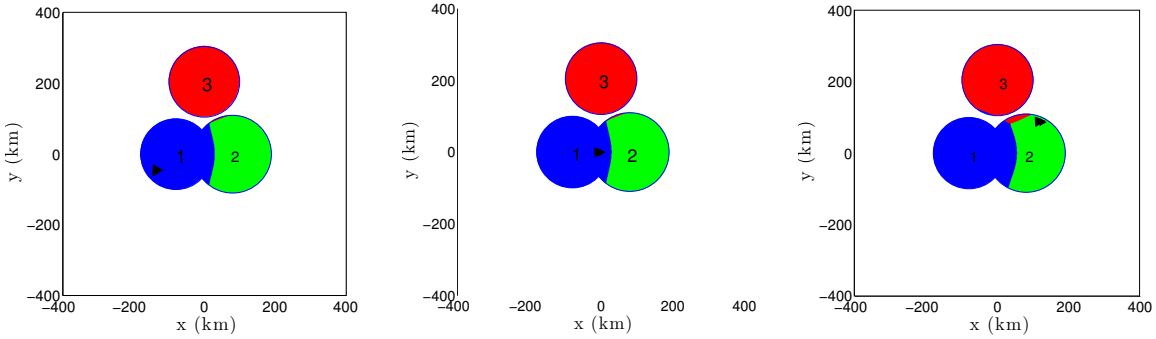

(a) t=60s (b) t=154s (c) t=248s

Figure 3.10: Multi-target assignment boundaries and track zones for the second of two targets, which change as a function of the first target's position (shown as black dot). The target velocity is 2.5 km/sec [68].

by a black dot. In Fig. 3.10(a), target $M = 1$ is being tracked by ship 1 located at (-100,0). In Fig. 3.10(b), the first target is approaching the $M = 1$ target assignment boundary and is still being tracked by ship 1. In Fig. 3.10(c), the first target has crossed the $M = 1$ target assignment boundary and is being tracked by ship 2, thus ship 2's track zone has decreased due to the resources expended to track the first target.

Chapter 4

Consensus-based Optimization and Validation in Three Dimensions

This chapter presents a distributed, consensus-based approach to optimize the radar resource allocation for ballistic missile surveillance and target tracking. Radar search and target tracking consume resources as described in the three-dimensional nonlinear physical radar model in Chapter 2. Target tracking includes an estimate of the resources required to reduce target state uncertainty to a desired level to support engagements. Each radar determines their preferred radar-to-target assignment using a probabilistic optimization algorithm that balances radar resource loading and minimizes the total radar usage as described in Section 4.2. Under heightened tracking demand, radar search resources may be reallocated to track as described in Section 2.1.2 and search sectors degrade symmetrically about a designated threat axis. A unique global radar-to-target assignment that is robust to resource estimation error is generated by a distributed consensus algorithm as described in Section 4.3.

4.1 Optimization Approach

A two-stage approach is implemented to solve the target-assignment problem. The first stage is a local optimization in which each radar finds a target-assignment solution for the entire network that balances radar usage between radars and min-

imizes the total amount of radar usage among all radars. Radar resource usage depends on the ballistic missile and air-defense search and track requirements as well as resources required to reduce target uncertainty for engagements. Minimizing total resource usage among each radar allows for additional resources to be applied to either search or track functions depending on the mission priorities as described by a resource-allocation doctrine. Because of the binary structure of solutions to the target-assignment problem (each target is assigned to exactly one radar), graph-theoretic methods described in Section 2.3 are used to represent the set of all possible target-assignment solutions. Due to the sheer number of candidate solutions that would have to be considered in an exhaustive search approach for a large raid scenario, a probabilistic optimization algorithm known as a genetic algorithm (GA) [8] is used to find the target-assignment solution that balances and minimizes the total radar resource usage. GA's maximize the fitness of a population of chromosome-like candidate solutions using crossover, mutation, and other evolution-inspired operations.

Two common approaches exist for multiple-objective optimization methods using genetic algorithms [69]. The first approach, which is the approach taken in this dissertation, combines the individual objective functions into a single composite function by selecting desired weights for each individual function. The second approach determines an entire set of solutions that are non-dominated with respect to each other. This set is known as a Pareto optimal set [69],[70]. Pareto optimal sets may be preferred to single solutions when weights are difficult to determine or if the trade-offs between each objective function are desired. However, the size of

the Pareto set increases with the number of objectives [70].

The second stage of the target-assignment problem requires inter-radar coordination. Radars repeatedly exchange and update their individual target-assignment solutions over a balanced and strongly connected communication network in an iterative fashion that yields consensus on a single global solution. By using a theoretically justified consensus control algorithm [9], the initial target-assignment solution identified by each radar will be updated in such a way so as to reach an agreement on a single solution.

The binary structure of the target-assignment solutions lends itself to a binary consensus algorithm [37], [71] which has the additional benefit of being formulated to be tolerant of communication noise and fading channels. Although reaching consensus on the optimal target assignment may not always be necessary, since the coordinating radars may all have access to the same optimization inputs, the additional stage of reaching consensus among coordinating radars ensures that the target-assignment process is robust to errors in resource estimation. These errors arise because of the dynamic nature of the search resource allocation in the presence of many targets—each radar may not know the search allocation of every other radar. Consensus also provides robustness to inaccurate or unaccounted for sensor biases, eliminates the possibility that a detected target is untracked when tracking resources are available, and ensures that all radars share the same target-assignment solution even in the presence of communication noise.

Using the radar and communication modeling framework outlined in Section 2.3 and the target-assignment optimization and consensus algorithm from Sec-

tions 4.2 and 4.3, respectively, Section 4.4 demonstrates the improvement in radar resource allocation and target tracking as compared to radars that are unable to coordinate on their target-assignment using Monte Carlo simulations.

4.2 Target Assignment Optimization

This section presents the target assignment optimization framework for multiple radars coordinating over a strongly connected, balanced communication network with possibly directed links. It is assumed that each radar can accurately estimate the position of every other radar using either GPS or other available sensors. All radars implement a linear target tracking filter that uses the target measurements in 2.13–2.18 to estimate the target state at each time step. Each radar broadcasts the target state and uncertainty over the radar communication network and uses this information in addition to an estimate of the other radars' search resource usage to optimize their target assignments. Because search resource usage is not usually broadcast, each radar must estimate the search resource usage of other radars.

A target-assignment solution is the set of radar-to-target pairings that assigns exactly one radar in the set $\mathcal{N}$ to each detected target in the disjoint set $\mathcal{M}$, represented by the adjacency matrix of the bipartite graph G_{track}. The framework of the target-assignment optimization problem is based upon meeting the following two objectives: (i) balancing radar resource tasking and (ii) minimizing total radar resource usage. Objectives (i) and (ii) are formulated using a quadratic form based on a weighted graph Laplacian [61] that reflects the priorities of balancing resource

usage verses total resource usage. The solution to the optimization problem is the target-assignment graph G_{track} that best achieves the convex combination of both objectives.

For even a small number of targets, the exact solution to the problem obtained by exhaustive search of each radar-to-target pairing yields excessive computational time requirements since the number of possible pairings is N^M. An alternate approach that achieves convergence to a near-optimal solution after considering dramatically fewer candidates is called a genetic algorithm (GA) [8]. A GA's basic principle is the maintenance of a population of individuals (genotypes) that evolve over time based on the laws of natural selection and genetic information recombination [72]. Each individual represents a feasible solution of an optimization problem, such as the target-assignment solution, and its objective function value is said to be its fitness which is to be minimized (or maximized). The input to a genetic algorithm is an initial population of randomly generated individuals. For each generation, every individual in the population is evaluated on their fitness, usually the value of the objective function in the optimization problem being solved. The more fit individuals are stochastically selected from the current population, and each individual's genome is modified to form a new generation. The algorithm terminates when either a maximum number of generations has been produced, or a satisfactory fitness level has been reached for the population. A general genetic algorithm is sketched in Table 4.1. While convergence results to the global optimal solution are proven in [73] and [74], these results assume an elitist selection strategy (the best individual survives with probability one). In [75], it is shown by means of homoge-

Table 4.1: Canonical Genetic Algorithm [75]

choose an initial population
determine the fitness of each individual
perform selection
repeat
    perform crossover
    perform mutation
    determine the fitness of each individual
    perform selection
until stopping criterion applies

neous finite Markov chains that canonical genetic algorithms never converge to the global optimum (though modified versions do).

A GA is used as opposed to alternatives like simulated annealing because the discrete genome-like candidate solutions of ones and zeros closely resemble an actual target-assignment pairing (i.e., the adjacency matrix of G_{track}). An initial population of potential target- assignment graphs is encoded as a binary solution as follows. Let $G_{track,k}$ be the target-assignment solution proposed by radar k for all radars and targets and let $A_k \in \mathbb{R}^{N \times M}$ be the adjacency matrix of $G_{track,k}$

such that

$$a_{ij} = \begin{cases} 1, & \text{if } G_{track,k} \text{ assigns target } j \text{ to radar } i \\ 0, & \text{otherwise.} \end{cases} \tag{4.1}$$

Note that A_k satisfies $\sum_{j=1}^{N} a_{jk} = 1$ which represents the constraint that each target is assigned to exactly one radar and no (detected) targets are unassigned. Each local target-assignment solution is evaluated based on the objective function described below. New target-assignment graphs (offspring) are produced from pairs of current graphs in the general population [76, pp. 211-231].

Objective (i) of the target-assignment optimization is to balance radar resources over the radar communication network G_{com}, (i.e., to minimize the differences in radar usage between all pairs of communicating radars). Let $P = [P_1\ P_2\ ...\ P_N]^T$ be the collection of all normalized (instantaneous) radar resource allocations, where $P_k \triangleq (T^{(tot)}_{search,k} + T^{(tot)}_{track,k} + T^{(tot)}_{eng,k} + \epsilon_k)/T_{max}$ denotes the total normalized resources used for search and track by radar k. Let L_{com} be the graph Laplacian of G_{com}. The optimal target-assignment network G_{track} balances radar tasking across G_{com} by minimizing the Laplacian quadratic form [12]

$$P^T L_{com} P \ = \sum_{(j,k)\in\mathcal{E}_{com}} (P_k - P_j)^2. \tag{4.2}$$

Note the sum in 4.2 is over all edges (j,k) in G_{com}. The quadratic form 4.2 represents the level of disagreement in the radar resource usage, provided G_{com} is a balanced and strongly connected communication network.

Objective (ii) of the target-assignment optimization problem is to minimize the total tracking resource usage over all radars in G_{com}. Minimizing tracking resource usage allows each radar to maximize the amount of resources available for BM track and AD search. Let I_N be the $N \times N$ identity matrix, which represents the Laplacian of a balanced graph consisting of only self-loops, i.e. $[l_{ij}] = 2$ for all $i = j$, and $[l_{ij}] = 0$ otherwise. (Note that a loop adds two to the degree matrix of a graph since a vertex with a loop "sees" itself as an adjacent vertex from both ends of the edge [61].) Minimizing total (squared) radar resources is equivalent to minimizing

the Laplacian quadratic form

$$P^T P = P^T I_N P. \tag{4.3}$$

Objectives (i) and (ii) are combined into a single multi-objective cost function by first normalizing each objective function by its maximum value and then forming a combined quadratic form. Let K be a weighting factor that represents the priority of balancing resource usage as compared to minimizing total resource usage. The overall cost function is the convex combination

$$J(G_{track}; G_{com}) \triangleq P^T \left[K \tfrac{2}{N^2(N-1)} L_{com} + (1-K)\tfrac{1}{N} I_N \right] P. \tag{4.4}$$

The target assignment solution that balances resource usage and minimizes total resources is

$$G^*_{track} = \underset{G_{track}}{\operatorname{argmin}} \left(J(G_{track}; G_{com}) \right). \tag{4.5}$$

A binary genetic algorithm [76, pp. 211-231] is used by each radar to compute the optimal target assignment G^*_{track} in 4.5. While the GA implementation ensures that every detected target is assigned to a radar (as long as resources are available), it does not ensure agreement between all radars on the optimal target-assignment. To prevent the situation where no radar claims responsibility for tracking a target or more than one radar tracks a single target, a consensus algorithm is employed to reach agreement on the optimal-target assignment.

4.3 Target Assignment Consensus

This section describes a consensus-based framework to reach agreement [9] on target assignment, as represented by the adjacency matrix of the target-assignment graph. Reaching consensus ensures exactly one common target assignment solution and avoids the possibility that a target is not tracked. The consensus algorithm described here also provides robustness to errors in radar resource estimation, track uncertainty improvements, and communication noise. A binary consensus algorithm is adopted, following [77] and [71], because of the binary nature of the target assignment solutions.

Let $G_{track,k}$ be the target assignment solution initially proposed by radar k using 4.5 and let $A_k \in \mathbb{R}^{N\times M}$ be the adjacency matrix of $G_{track,k}$ as in 4.1. Define $\bar{A}_k \in \mathbb{R}^{NM\times 1}$ to be the elements of A_k taken column-wise and arranged as a single column. $\bar{A}_k$ must be transmitted as a digital signal by radar k over G_{com}, which despite being balanced and strongly connected, may corrupt each transmission with receiver noise. Let $q_{jk}(n) \in \mathbb{R}$ represent the receiver noise at the nth time step in the transmission of the target assignment solution from the kth radar to the jth one. Because receiver noise typically has a flat power spectral density over the signal band and a zero mean Gaussian voltage distribution [78, p. 946], the receiver noise $q_{jk}(n)$ is assumed to be additive and zero-mean Gaussian with constance variance $\sigma_{jk}^2 = \sigma_w^2$. (Each radar also has the same constant noise variance since identical radars are considered, however the results also apply to varying and heterogenous noise variances [77].)

Let $\hat{A}_{jk}(n)$ represent the reception of the target assignment at the jth radar from the transmission of the kth one at the nth timestep, i.e., $\hat{A}_{jk}(n) = \bar{A}_k(n) + q_{jk}(n)$, if $(j,k) \in \mathcal{E}_{com}$, where $\mathcal{E}_{com}$ represents the set of radars in the edge set of G_{com}. Let $\mathcal{N}_j$ represent the set of radars k that can communicate with radar j (including itself) and $|\mathcal{N}_j|$ be the size of $\mathcal{N}_j$. Let $\text{Dec}(\cdot)$ denote a decision function for the binary 0-1 entry performed on each element such that $\text{Dec}(x) = 1$ if $x \geq 0.5$ and 0 otherwise. Each radar updates its own copy of the target assignment solution based on the received information as follows [77]:

$$\bar{A}_j(n+1) = \text{Dec}\left(\frac{1}{1+|\mathcal{N}_j|}\left[\bar{A}_j(n) + \sum_{k\in\mathcal{N}_j, k\neq j}(\bar{A}_k(n) + q_{jk}(n))\right]\right). \tag{4.6}$$

Note that 4.6 has the form of the consensus algorithm in 2.34, with $x = \bar{A}$, $\epsilon = 1/(1+|\mathcal{N}_j)|$, and $L_{com} = L$. The advantage of working with binary consensus as opposed to Euclidean consensus is that each node will reach consensus in finite time verses infinite time. A noisy network is in accurate consensus at time step n if each radar's updated copy of the target assignment solution is equal to the noise-free solution.

As shown in [77] and [71], the binary consensus algorithm 4.6 may be modeled as a Markov Chain, where the transitional probabilities from one state to the next are independent of the earlier states. Due to the presence of noise, there is no guarantee in reaching or staying in consensus since the steady-state behavior is independent of the initial state. However, the network can still achieve accurate consensus for a certain period of time depending on the size of the network and the

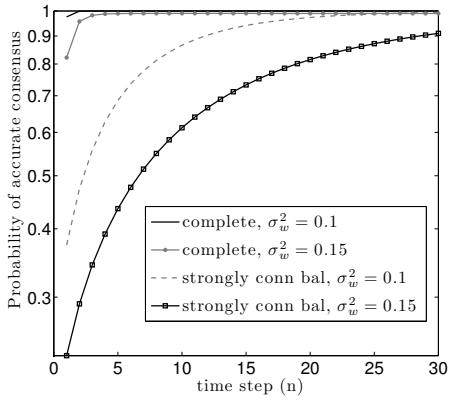

Figure 4.1: Consensus behavior with $N = 4$ radars and $M = 100$ targets for different noise variances, comparing a complete (all-to-all) communication network with a strongly connected and balanced communication network.

noise variance. For example, in either the case of zero noise variance (i.e. $\sigma_w^2 = 0$) or in the limit $N \to \infty$, a complete (all-to-all) network will reach consensus in one step and stay there [71]. In the case of non-zero noise variance ($\sigma_w^2 \neq 0$) and N finite, the probability of accurate consensus depends on N, σ_w, and the number of time steps (but not the initial conditions).

Fig. 4.1 compares the consensus behavior of a complete network and a strongly connected and balanced network for noise variances $\sigma_w^2 = 0.1$ and $\sigma_w^2 = 0.2$. Even for $\sigma_w^2 = 0.15$, which is larger than typically expected in receivers used for BM and AD applications, we observe a 99% probability that all radars reach and remain in agreement after four time steps in a complete network and after twenty time steps for a strongly connected balanced network, which represents a very small amount of data to be transmitted (approximately 700 bytes per radar).

Table 4.2: Multifunction array radar values used in simulations [45]

Radar Parameter	**Description**	**Value**
P_t	Peak transmitted power (MW)	4
P_{avg}	Average transmitted power (kW)	10
σ	Target radar cross section (RCS) m^2	1.0
A_e	Effective Antenna Aperture (m^2)	17.8
T_0	Standard temperature (degrees K)	290
F_n	Receive noise figure (dB)	6
L_s	Total system losses (dB)	12
G	Antenna gain (dB)	43.4
λ	Wavelength (mm)	0.1

4.4 Performance Validation

Using the radar and communication modeling framework outlined in Chapter 2, the improvement in radar resource allocation and target tracking as compared to radars that are unable to coordinate on their target-assignment is demonstrated using Monte Carlo simulations. Two different scenarios with four identical radars, i.e. $N = 4$, are considered in which each radar maintains a pulse-repetition-frequency of 100 update beams per second and performs volumetric searches over BM sectors optimized about the predicted target trajectories. Target measurements are updated every $T = 2$ seconds; radars optimize the target-assignment solution and reach consensus every 4 seconds over a network with a communication latency of $T_{com} = 6$ seconds. For all search sectors, a maximum five-second search revisit rate is instructed. The desired track uncertainty for engagement is 14.2 km which is less than 0.15 seconds of error for a BM target traveling at 200 km/s [45]. Table I lists the radar parameters used for both scenarios [45].

The target launch rate $p(k)$ is modeled as a Poisson distribution $p(k) = (\lambda^k/k!)e^{\lambda}$, where λ is the expected number of targets launched every $T = 2$ seconds and $p(k)$ is the probability that $k = 0, 1, 2, ...$ targets will be launched every T seconds. BM raid size mean and standard deviation are shown in Fig. 4.2 for increasing values of launch rate λ. Targets are detected with a single–look probability of detection of 0.9 after they penetrate one of the ballistic missile search sectors [4]. Coordinated radars broadcast the target state and uncertainty over the radar communication network G_{com} shown in Fig. 2.9, solve for optimal target-assignment using 4.5, and use this solution to initialize the binary consensus algorithm 4.6. The consensus algorithm uses G_{com} with noise variance $\sigma_w^2 = 0.1$.

Coordinated radars are compared with two types of uncoordinated radars: Independent radars and Shared radars [79]. In the Independent case, each radar only tracks targets that are detected within its own search sector. In the Shared case, each radars may track a target detected by a neighboring radar but radars do not optimize the target assignment. Thus in the Shared case more than one radar may track the same target.

4.4.1 Scenario 1: Short-range BM Raid

The first scenario considers a short range (< 500 km) BM raid. Each target has maximum life span of 300 seconds and vanishes on impact. Targets trajectories are chosen from a set of four launch points and two aim points with a larger percentage of the targets coming from the two launch points located near (0,0) as shown in

Fig. 4.3. Fig. 4.3 also plots the location of each radar with respect to the aim points

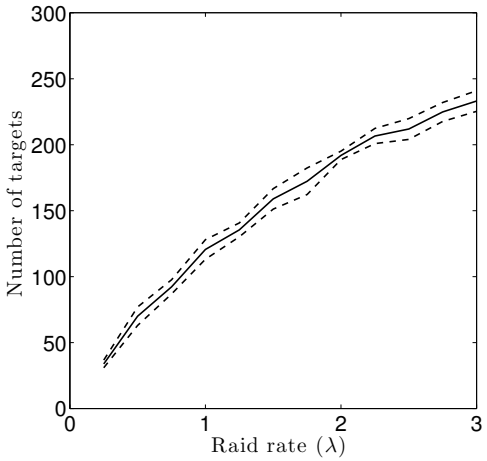

Figure 4.2: The total number of launched targets (mean and standard deviation) increases with the raid rate λ (expected number of targets launched every $T = 2$ seconds).

(denoted by the black X's). The ellipses around the aim points describe the 2σ ellipses of the impact point probability distribution.

Figs. 4.4(a), 4.4(c), and 4.4(e) plot the mean-centered standard deviation of the total normalized resource usage obtained from 30 Monte Carlo trials with a variable resource allocation doctrine, a launch rate of $\lambda = 0.5$, and $K = 0.5$. This value of K implies minimizing radar resource usage has the same priority as balancing resource usage. (Recall a variable resource allocation doctrine implies that once resources initially reserved for BM track are depleted, AD search resources may be converted to BM track.) In this case the remaining AD search resources are re-optimized to ensure that the search sector is centered on the expected AD threat axis. Note that on average, Coordinated radars use less total resources than both the Independent and Shared radars throughout the scenario. Figs. 4.4(b), 4.4(d), and 4.4(f) plot the total pairwise difference in radar usage for all three cases. Throughout the entire

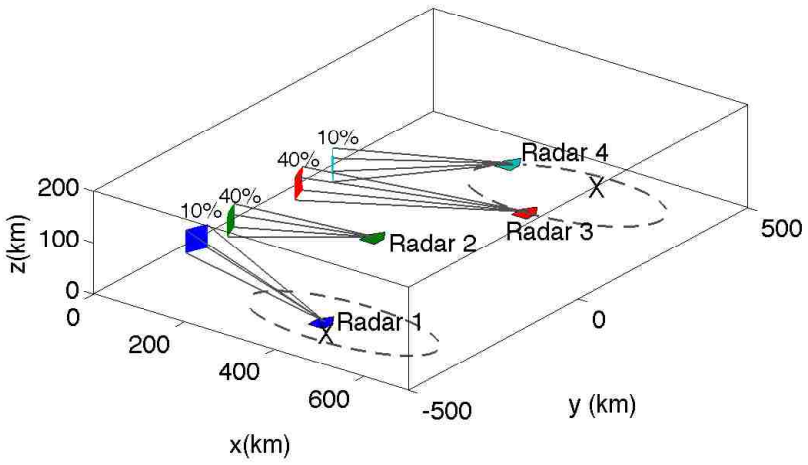

Figure 4.3: Scenario 1 radar locations and BM search sectors with respect to the target launch and impact point distributions.

scenario, the maximum pairwise difference for Coordinated radars is less than the maximum pairwise difference for both Independent and Shared radars, indicating superior load balancing as compared to the uncoordinated alternatives. Figs. 4.5(a)–4.5(b) plot the maximum mean value of the total normalized radar resource usage and the mean of the sum of pairwise differences in resource usage for Coordinated radars over a range of launch rates λ and gains K. Note that smaller values of K result in less total resource usage as compared to larger values of K, which result in a more balanced resource utilization as expected. To highlight the benefit of coordination in terms of reducing the number of missed targets, Figs. 4.5(c)–4.5(f) plot the mean-centered standard deviation (grey bar) and single radar worst-case (dotted-line) total resource usage and sum of pairwise difference in resource usage statistics from the Monte Carlo simulations for all raid rates and a fixed value $K = 0.6$ for both

Coordinated and Independent radars. (Shared radars are not plotted since their maximum resource usage is equal to one for all raid rates.) While the Independent radars are observed to use less average resources due to their lack of coordination, their resource usage is unbalanced across the network and leads to a greater number of missed targets as shown in Table 4.3.

Table 4.3: Scenario 1: Total Number of Missed Targets for $K = 0.5$

	$\lambda = 0.5$	$\lambda = 1.0$	$\lambda = 1.5$	$\lambda = 2.0$
Coordinated	0	0	1	14
Independent	0	0	4	38
Shared	11	51	79	94

4.4.2 Scenario 2: Medium-range BM Raid

The second scenario considers a raid of medium range ($\approx$ 1500 km) ballistic missiles. Radars are stationed farther from the launch points and impact points as compared to Scenario 1 (see Fig. 4.6). The goal of this scenario is to stress the resource requirement for both tracking and engagements due to the increased target range from each radar. While each target has a total life expectancy of 600 seconds, targets are tracked until they reach apogee altitude at 350 km and the total scenario time is limited to 200 seconds due to radar resource saturation. Targets trajectories are chosen from the same set of four launch points and two different aim points with a larger percentage of the targets coming from the two launch points located near (0,0). Fig. 4.6 also plots the location of each radar with respect to the aim points (denoted by the black X's). The ellipses around the aim points describe the

2σ ellipses of the impact point probability distribution.

Similar resource usage trends in Scenario 2 are observed for 30 Monte Carlo trials with a variable resource allocation doctrine, a launch rate of $\lambda = 0.5$, and $K = 0.5$. Figs. 4.7(a), 4.7(c), and 4.7(e) illustrate that Coordinated radars use less total resources than both the Independent and Shared radars throughout the scenario. As with Scenario 1, the total pairwise difference in radar usage for Coordinated radars is less than the maximum pairwise difference for both Independent and Shared radars as shown in Figs. 4.7(b), 4.7(d), and 4.7(f), indicating superior load balancing.

Figs. 4.8(a)–4.8(b) show that resource usage in the longer range BM raid is highly dependent on the gain K. A smaller value of K reduces the total resource usage as compared to larger values of K, which result in a more balanced resource utilization. Coordinated radars also display superior worst case resource usage as shown in Figs. 4.8(c)–4.8(f) for all raid rates and a fixed value $K = 0.5$. In terms of missed number of targets, Table 4.4 highlights that Coordinated radars track more targets than Independent and Shared radars in a medium-range BM raid scenario.

Table 4.4: Scenario 2: Total Number of Missed Targets for $K = 0.5$

	$\lambda = 0.5$	$\lambda = 1.0$	$\lambda = 1.5$
Coordinated	0	2	21
Independent	3	16	39
Shared	24	39	72

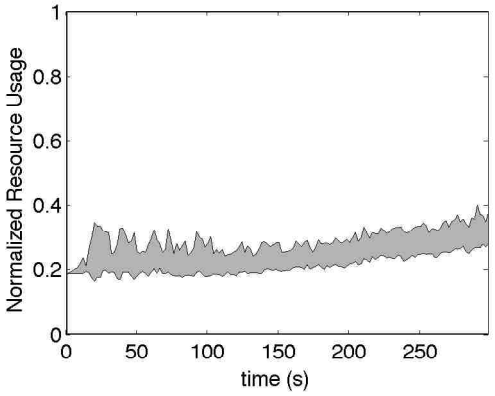

(a) Coordinated total resource

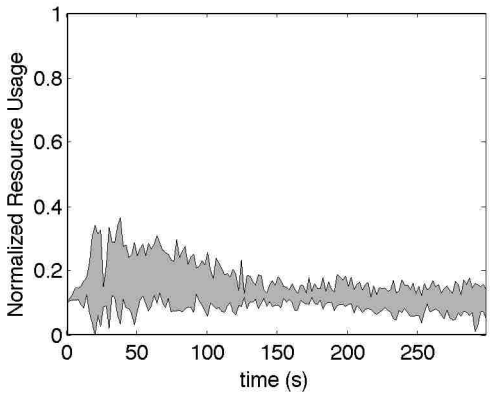

(b) Coordinated sum of pairwise difference

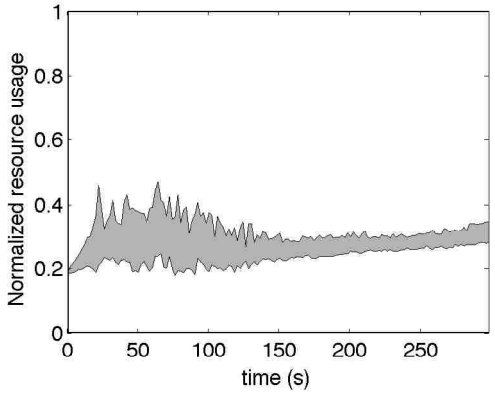

(c) Independent total resource

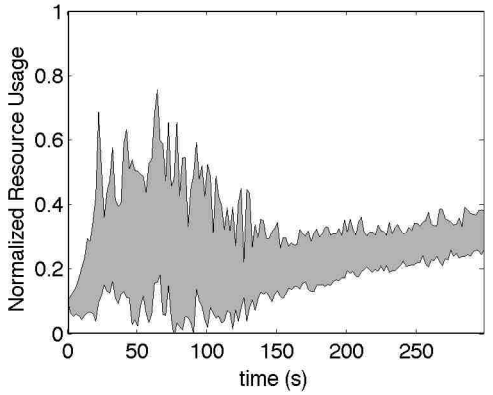

(d) Independent sum of pairwise difference

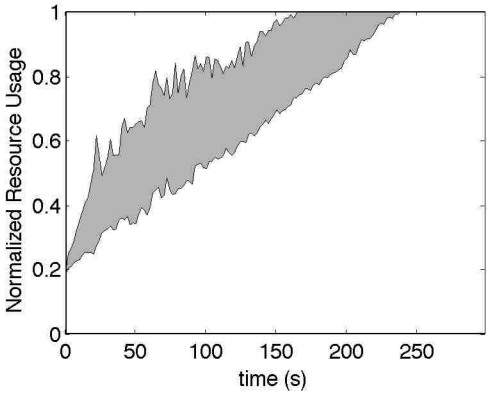

(e) Shared total resource

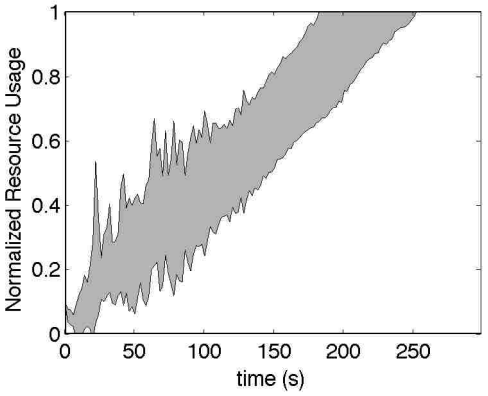

(f) Shared sum of pairwise difference

Figure 4.4: Scenario 1 resource usage statistics for $\lambda = 0.5$ targets every 2 seconds and $K = 0.5$. Coordinated radars use less total resources and stay more balanced in radar resource usage as compared to Independent and Shared radars

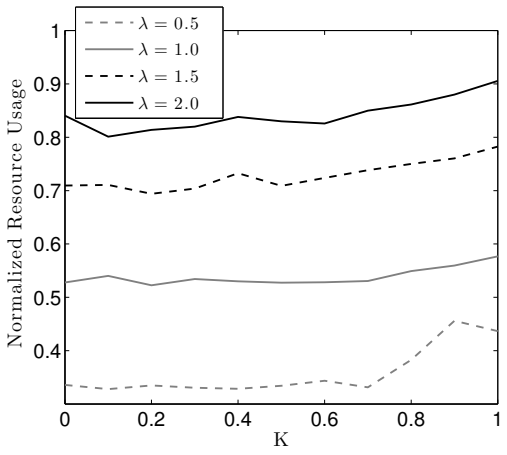

(a) Coordinated total resource

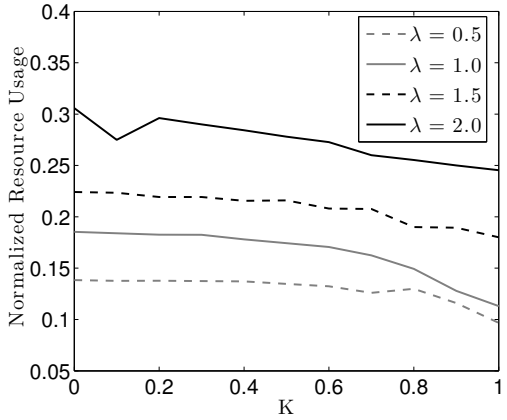

(b) Coordinated sum of pairwise difference in resource

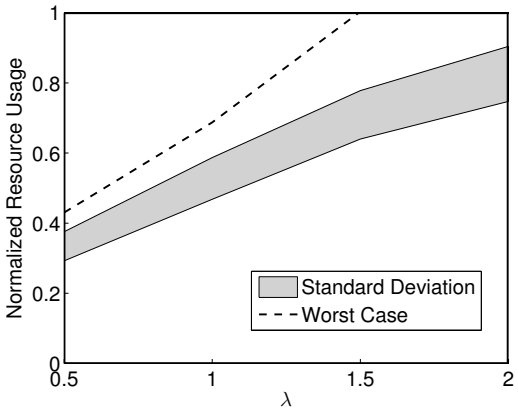

(c) Coordinated total resource

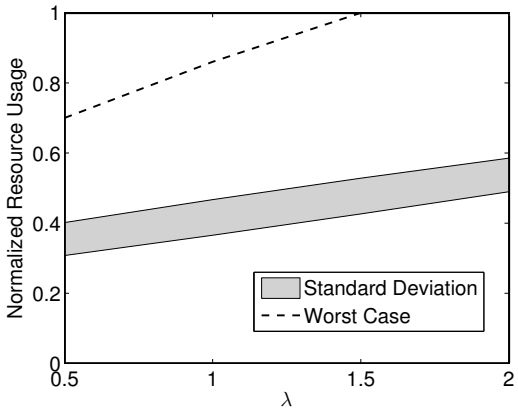

(d) Independent total resource

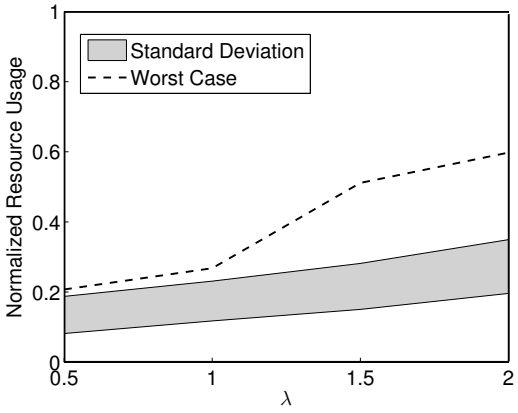

(e) Coordinated sum of pairwise difference in resource

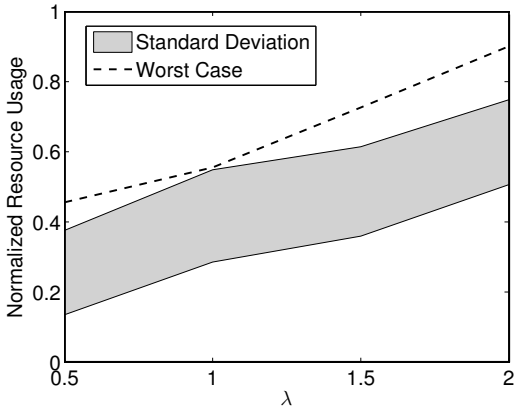

(f) Independent sum of pairwise difference in resource

Figure 4.5: (a)–(b) illustrate the total resource usage and sum of pairwise resource usage dependence on gain K for all raid rates λ; (c)–(f) highlight the increase total resource usage and the sum of the pairwise difference in resource usage with larger raid rates. Note that, regardless of the raid rate, the worst case radar usage for Coordinated radars is less than Independent and Shared radars (not shown).

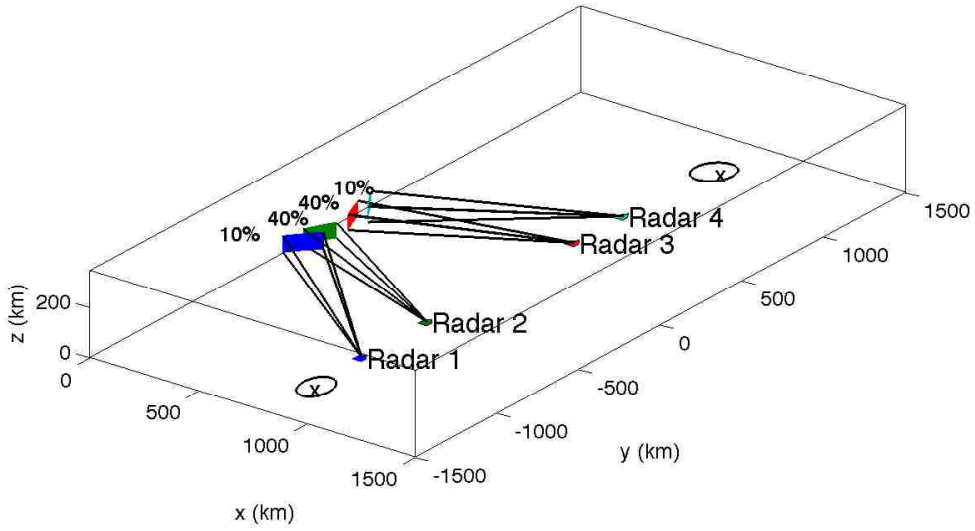

Figure 4.6: Radar locations and BM search sectors with respect to the target launch and impact point distributions.

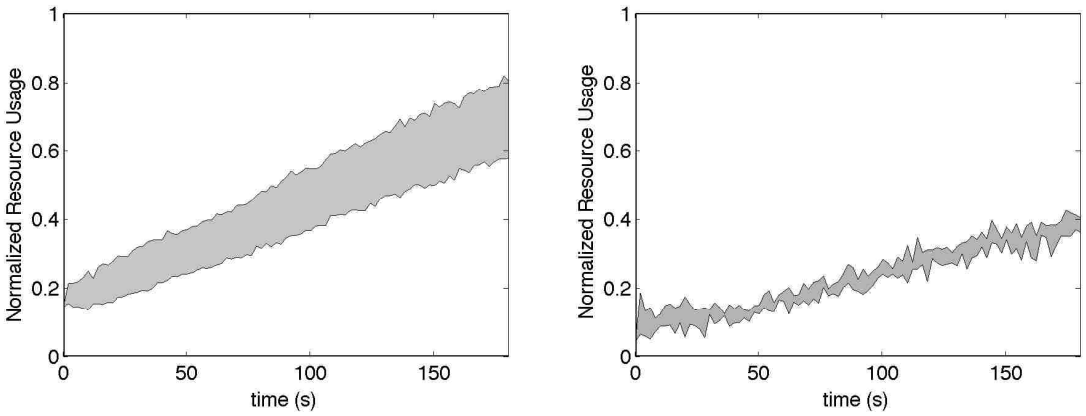

(a) Coordinated total resource

(b) Coordinated sum of pairwise difference

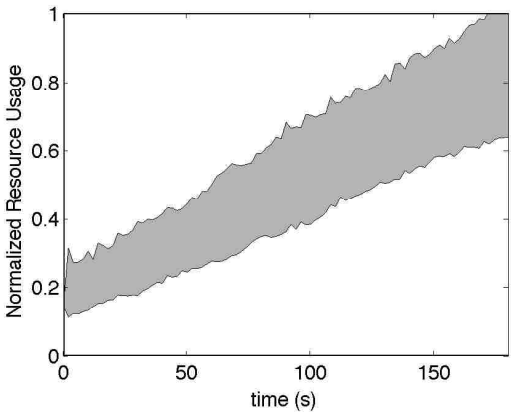

(c) Independent total resource

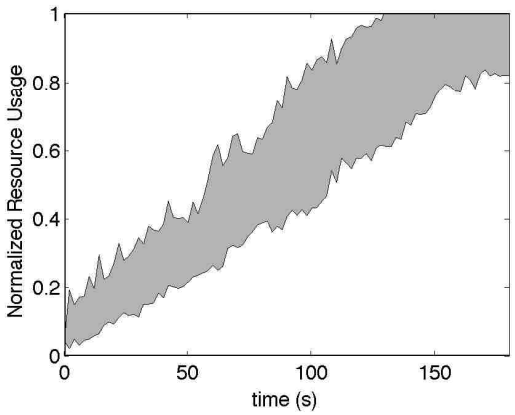

(d) Independent sum of pairwise difference

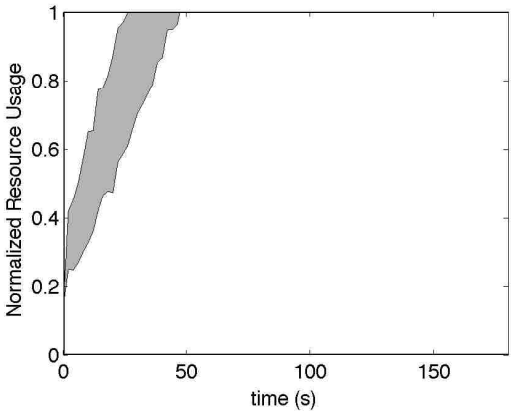

(e) Shared total resource

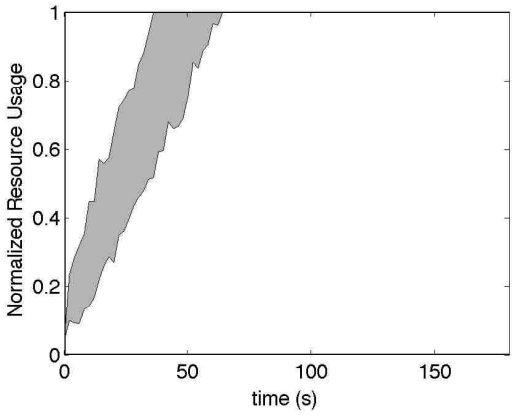

(f) Shared sum of pairwise difference

Figure 4.7: Scenario 2 resource usage statistics for $\lambda = 0.5$ targets every 2 seconds and $K = 0.5$. Coordinated radars use less total resources and stay more balanced in radar resource usage as compared to Independent and Shared radars

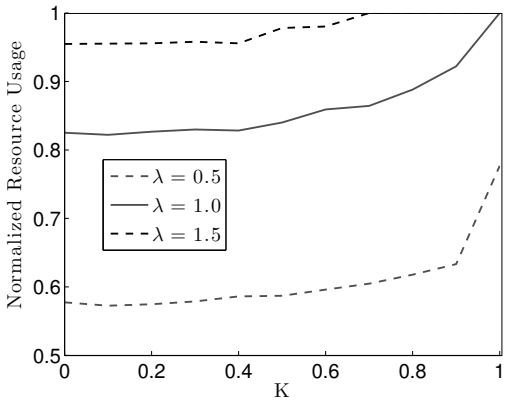

(a) Coordinated total resource

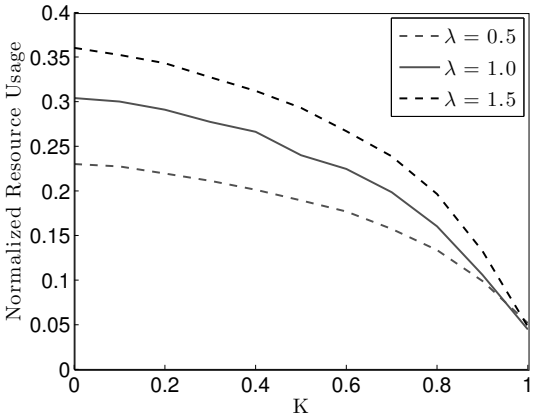

(b) Coordinated sum of pairwise difference in resource

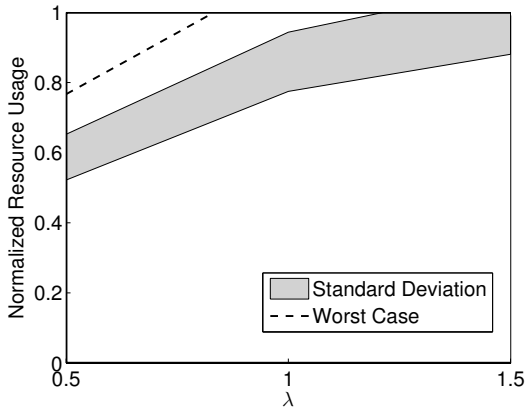

(c) Coordinated total resource

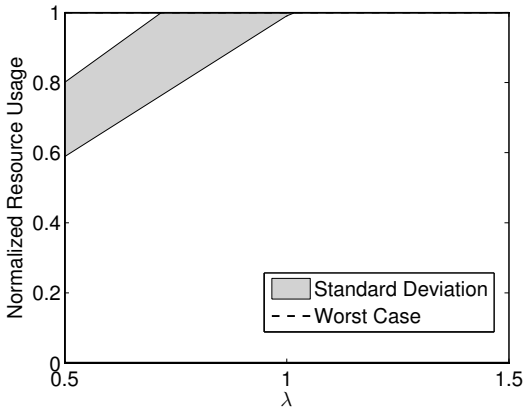

(d) Independent total resource

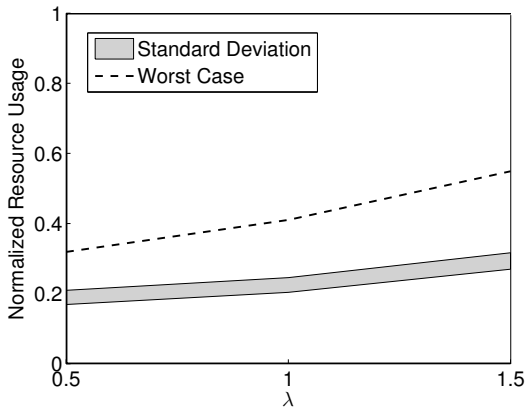

(e) Coordinated sum of pairwise difference in resource

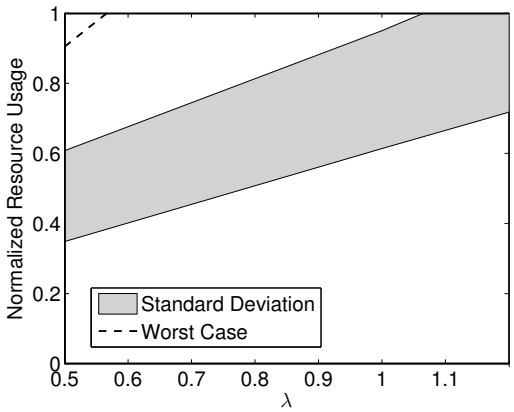

(f) Independent sum of pairwise difference in resource

Figure 4.8: (a)–(b) illustrate the total resource usage and sum of pairwise resource usage dependence on gain K for all raid rates λ; (c)–(f) highlight the increase total resource usage and the sum of the pairwise difference in resource usage with larger raid rates. Note that, regardless of the raid rate, the worst case radar usage for Coordinated radars is less than Independent and Shared radars (not shown).

Chapter 5

Conclusions

5.1 Summary of Dissertation

Distributed optimization of radar resource allocation addresses the problem of effectively managing the limited resources among a networked multifunction radars to accomplish a prioritized list of search and track functions. This dissertation has contributed to the design of a conceptual architecture and framework for the distributed resource coordination of multifunction radar systems.

Starting with two-dimensional linear and nonlinear radar models, a distributed search-area optimization algorithm is described that maximizes the collective search area of identical shipboard multifunction radar systems in which some or all of the systems are able to coordinate on their tasking. Analytical results show that the search-area optimization algorithm increases the combined search area of two and three ships over the uncoordinated combined search area in a directed network modeled using graph theory. An optimal target-assignment algorithm is presented that balances the radar tasking for radars that are both optimized and unoptimized with respect to their search area. For radars that coordinate on their target assignment, the solution to the target assignment problem is a hyperbolic boundary determined by the radar surveillance requirements, range to the target, and current target tasking. The proposed solutions are validated by a combination of analytical

and numerical results using a simulated annealing algorithm.

Using a three-dimensional nonlinear radar model, a distributed, consensus-based optimization approach to manage radar resources is described for ballistic missile and air-defense surveillance and target tracking. A target-assignment optimization algorithm that uses a binary genetic algorithm to balance and minimize radar resource usage across the radars in the network is presented. Radar resources include the additional resources required to reduce track uncertainty in support of engagements. Remaining air-defense search resources are optimized about a projected threat-axis by employing a simulated annealing algorithm. Radar reach agreement on the optimal target-assignment using a binary consensus algorithm. Monte Carlo simulations demonstrate that the consensus-based distributed target-assignment approach uses less overall resources and remains more balanced in resource usage than uncoordinated alternatives, thus increasing the number of additional targets that may detected and tracked.

5.2 Suggestions for Future Research

Optimization of sensor resource management can lead to many different approaches and tradeoffs. While this dissertation has advanced the state of the art in multifunction radar resource coordination for ballistic missile and air-defense surveillance and target tracking, it has also highlighted various focus areas for future work.

The 3D nonlinear radar model considered in Chapter 2 can be improved in fidelity by considering radar power requirements as an additional dynamic resource

constraint and tradeoff [80]. Maneuvering targets would add another level of complexity to the target-assignment optimization problem as additional tracking resources would be required to increase the target measurement update rate to maintain a desired level of track accuracy [81], [82]. Additional tracking considerations such as including imperfect data associations [57],[83] and tracking in clutter are expected to affect the track uncertainty, however accurately translating these additional considerations to a radar time-resource loading requirement requires additional research [80] . Certainly the more complicated the threat environment, the more adaptable and robust the radar resource manager must be to determine the proper resource to task allocation in order to maintain an accurate situational awareness picture.

The dynamic load balancing and load minimization approach has demonstrated improved performance over the uncoordinated alternative strategies for BM target tracking and to a lesser extent air-defense surveillance. However, these functions represent only two of the many functions that a multifunction radar systems performs. Indeed the greatest benefit of the radar itself is its ability to perform many different functions that previously required separate radars. To that end, the balancing and minimizing approach could be extended to tracking air- and surface targets as well as long-range search. Radar functions such as track initiation, target discrimination, and engagement assessment are functions that were not considered as part of this thesis but may consume a large amount of radar resources depending on the mission and tasking priorities. Optimizing the sensor placement to balance and minimize the radar resource usage for search and anticipated target tracking

seems to be another relevant extension of our existing work.

The implementation of the target-assignment optimization algorithm presented in this dissertation can be improved. The genetic algorithm provides a computationally efficient method to solve for a local optimal solution in a significantly reduced timeframe as compared to an exhaustive search. However, there may exist alternative optimization algorithms that converge to a global optimal solution in less time than the genetic algorithm implemented here. While all the computations required for the Monte Carlo simulations were performed on a standard laptop computer, the target models and threat environment were less complex than would be observed in reality. Thus using real target and radar data would be of benefit to compare the computational performance of the target-assignment optimization algorithm within the framework of radar's data processing timeline and communication latency.

Consideration of non-homogenous radars should be a next step in furthering this research. Sensors other than radars that can provide an estimate of their resource usage for surveillance and target tracking should also be considered and would provide a logical extension of the existing radar modeling framework.

Appendix A

Search-Area Maximization Analytical Results

For completeness the proofs of the Lemmas 1–9 from Section 3 are presented.

Proof of Lemma 1

Since $f(\rho)$ monotonically increases with ρ and $\alpha > 0$, then ρ^* satisfies 3.6=0.

□

Proof of Lemma 2

The distance between the two ships as a function of the search radius ρ and angle of overlap θ is found by solving 3.10 for δ to obtain

$$\delta^* \approx \rho\left(2 - \frac{\theta^2}{4}\right). \tag{A.1}$$

Using 3.11, the optimality condition $g(\rho^*, \delta^*) = 0$ is satisfied when

$$\theta = \frac{\alpha\rho^* + \beta}{a}. \tag{A.2}$$

Substituting A.2 into A.1 yields 3.13.

Since 3.8 is maximized for small values of θ, a Taylor series expansion of $\sin\theta$

about $\theta = 0$ is performed in 3.8, which yields

$$f(\rho, \delta) \approx 2\pi\rho^2 - \frac{\theta^3\rho^2}{6}. \tag{A.3}$$

The derivative of A.3 with respect to ρ is

$$\frac{\partial f}{\partial \rho} = 4\pi\rho - \frac{1}{3}\theta^3\rho - \frac{1}{2}\rho^2\theta^2\frac{\partial \theta}{\partial \rho}. \tag{A.4}$$

A.4 is written in terms of ρ using A.2 and $\partial\theta/\partial\rho = \alpha/a$. The final equation is a quartic function in ρ with a degenerate root equal to 0, leaving the cubic polynomial 3.12. As a consequence of the intermediate value theorem [84], 3.12 has at least one solution among the real numbers because the degree of the polynomial is odd. Because its discriminant

$$\Delta = 18b_1b_2b_3b_4 - 4b_3^3b_1 + b_3^2b_2^2 - 4b_4b_2^2 - 27b_4^2b_1^2 \tag{A.5}$$

is positive, there exists three real roots. The largest root is chosen to maximize A.3, which completes the proof. □

Proof of Lemma 3

From Lemma 2, the objective function is given by A.3 where $\theta = (\alpha\rho^* + \beta)/a$ as in A.2 for the optimality condition $g(\rho^*, \delta) = 0$. Substituting A.2 into A.1 with

$\delta^* = \delta$ yields

$$\delta \approx \rho^* \left(2 - \left(\frac{\alpha\rho^* + \beta}{2b} \right)^2 \right). \tag{A.6}$$

Solving A.6 for ρ^* yields 3.12, which completes the proof. □

It was shown in Lemma 3 that given the position of two ships with equal radii, one can solve for the maximum search radius for each radar. Note that in order to satisfy the optimality condition $g(\rho^*, \delta) = 0$, each ship position must satisfy A.6 for at least one real root ρ^*. Choosing $\delta \leq 2\rho_1$ where $\rho_1 = \rho^*$ from the optimal $N = 1$ search radius ensures a solution to A.6.

Proof of Lemma 4

Let $\rho_1 = \rho^*$ (the $N = 1$ optimal radius). The objective function is given by 3.24, where $\theta_{1,2}$ and $\theta_{2,1}$ are as in 3.19 and 3.20 respectively and $\delta_{1,2} = \delta \leq 2(\rho^* + \rho_2)$. To satisfy the $N = 2$ sensor overlap requirement and to avoid solving first for δ^*, δ is chosen such that $\delta \leq 2\rho^*$. 3.24 is maximized when

$$\alpha\rho_2 + \beta - 2a\sqrt{2\left(1 - \frac{\delta^2 - \rho^{*2} + \rho_2^2}{2\delta\rho_2}\right)} = 0. \tag{A.7}$$

Solving A.7 for ρ_2 yields 3.26, which completes the proof. □

Proof of Lemma 5

Since each ship is equally spaced with equal radar search radii, the optimal distance δ^* is found by solving 3.11 for the optimality condition $g(\rho^*, \delta^*) = 0$.

Substituting A.2 into A.1 yields A.6. The combined search area given by 3.27 can be expressed as

$$f(\rho, \delta) = \left(\frac{3}{2}\pi - \theta + \sin\theta\right) 2\rho^2, \tag{A.8}$$

where $\theta_{1,2} = \theta_{2,1} = \theta_{2,3} = \theta_{3,2} = \theta$ and $\theta_{1,3} = \theta_{3,1} = 0$ (since shipboard radars 1 and 3 do not overlap in coverage area). A.8 is maximized for small overlap angle θ, thus a Taylor series expansion of $\sin\theta$ is performed about $\theta = 0$ in A.8 to obtain

$$f(\rho, \delta) \approx 3\pi\rho^2 - \frac{\theta^3\rho^2}{3}. \tag{A.9}$$

Taking the derivative of A.9 with respect to ρ yields

$$\frac{\partial f}{\partial \rho} = 6\pi\rho - \frac{2}{3}\theta^3\rho - \rho^2\theta^2\frac{\partial\theta}{\partial\rho}. \tag{A.10}$$

A.10 is written in terms of ρ using $\theta = (\alpha\rho^* + \beta)/a$ and $\partial\theta/\partial\rho = \alpha/a$. The final equation is a quartic function of ρ with a degenerate root equal to 0, leaving the cubic polynomial 3.12 with its discriminant A.5 greater than zero. Thus there exists three real roots and the largest root is chosen to maximize A.9, which completes the proof. □

Proof of Lemma 6

From Lemma 5, the objective function is given by A.9 where $\theta = (\alpha\rho^* + \beta)/a$ as in A.2 for the optimality condition $g(\rho^*, \delta) = 0$. Substituting A.2 into A.1 with $\delta^* = \delta$ yields A.6. Solving A.6 for ρ^* yields 3.12, which completes the proof. □

Proof of Lemma 7

As in Lemma 4, let $\rho_2 = \rho^*$ from Lemma 1. Then

$$\theta_{1,2} \approx 2\sqrt{2\left(1 - \frac{\delta^2 + {\rho_1}^2 - {\rho^*}^2}{2\delta\rho_1}\right)} \tag{A.11}$$

$$\theta_{2,1} \approx 2\sqrt{2\left(1 - \frac{\delta^2 + {\rho^*}^2 - {\rho_1}^2}{2\delta\rho^*}\right)} \tag{A.12}$$

$$\theta_{2,3} \approx 2\sqrt{2\left(1 - \frac{\delta^2 + {\rho^*}^2 - \rho_3^2}{2\delta\rho^*}\right)} \tag{A.13}$$

$$\theta_{3,2} \approx 2\sqrt{2\left(1 - \frac{\delta^2 + {\rho_3}^2 - {\rho^*}^2}{2\delta\rho_3}\right)}. \tag{A.14}$$

The combined search area 3.27 becomes

$$\begin{aligned} f(\rho_1, \rho_2, \rho_3, \delta) &= \left(\pi + \left(\frac{\sin\theta_{1,2} - \theta_{1,2}}{2}\right)\right)\rho_1^2 \\ &+ \left(\pi + \left(\frac{\sin\theta_{2,1} - \theta_{2,1}}{2} + \frac{\sin\theta_{2,3} - \theta_{2,3}}{2}\right)\right)\rho_2^2 \\ &+ \left(\pi + \left(\frac{\sin\theta_{3,2} - \theta_{3,2}}{2}\right)\right)\rho_3^2. \end{aligned} \tag{A.15}$$

A.15 is maximized when the overlap angle for each ship pair, $\theta_{j,k}$, is small, thus a Taylor series expansion of $\sin\theta_{j,k}$ is performed about $\theta_{j,k} = 0$ in A.15 to obtain

$$\begin{aligned} f(\rho_1, \rho_2, \rho_3, \delta) &\approx (2\pi - \frac{\theta_{1,2}^3}{6})\frac{\rho_1^2}{2} + (2\pi - \frac{\theta_{2,1}^3}{6} - \frac{\theta_{2,3}^3}{6})\frac{{\rho^*}^2}{2} \\ &+ (2\pi - \frac{\theta_{3,2}^3}{6})\frac{\rho_3^2}{2}. \end{aligned} \tag{A.16}$$

It follows from Lemma 4 that A.16 is maximized for the optimality condition $g(\rho_k, \delta) = 0$. Given the spacing δ between each adjacent ship pair and $\rho_2 = \rho^*$,

A.11 is solved for ρ_1 and A.14 for ρ_3 with $\theta_{1,2} = (\alpha\rho_1 + \beta)/a$ and $\theta_{3,2} = (\alpha\rho_3 + \beta)/a$, which yields 3.26 and completes the proof. □

Proof of Lemma 8

For Scenario 2 there exists no common overlap area for all three radars. In addition, since all radars have equal radii and separation, the overlap angles between each radar pair, $\theta_{j,k}$, are equal, i.e. $\theta_{1,2} = \theta_{2,1} = \theta_{2,3} = \theta_{3,2} = \theta_{1,3} = \theta_{3,1}$. The combined search area 3.27 is expressed as

$$f(\rho, \delta) = 3\pi\rho^2 - 3\theta\rho^2 + 3\sin\theta\rho^2, \tag{A.17}$$

where θ equals the total overlap angle for each individual ship, i.e., $\theta_1 = \theta_{1,2} + \theta_{1,3}$ and $\theta_1 = \theta_2 = \theta_3 = \theta$. A.17 is maximized when the overlap angle for each ship pair is small, thus a Taylor series expansion of $\sin\theta$ is performed about $\theta = 0$ in A.17 to obtain

$$f(\rho, \delta) = 3\pi\rho^2 - \frac{\theta^3\rho^2}{2}. \tag{A.18}$$

The distance between each ship pair is expressed as a function of the search radius ρ and pairwise angle of overlap $\theta_{j,k}$ by solving 3.10 for δ. Using 3.11, the optimality condition $g(\rho^*, \delta) = 0$ is satisfied for A.2, where θ is the sum of each pairwise angle of overlap, i.e. $\theta_1 = \theta_{1,2} + \theta_{1,3} = 2\theta_{1,2}$. Substituting $\theta/2$ into A.6 yields 3.12 and completes the proof. □

Proof of Lemma 9

The optimal distance between all three ships follows from Lemma 2 and Lemma 8. Taking the derivative of A.18 with respect to ρ yields

$$\frac{\partial f}{\partial \rho} = 6\pi\rho - \theta^3\rho^2 - \frac{3}{2}\theta^2\rho^2\frac{\partial \theta}{\partial \rho}. \tag{A.19}$$

A.19 is written in terms of ρ using A.2 with $\partial\theta/\partial\rho = \alpha/a$ The rest of the proof follows the proof of Lemma 2. □

Bibliography

[1] (2006, July). [Online]. Available: http://news.bbc.co.uk/2/hi/asia-pacific/5152918.stm

[2] [Online]. Available: http://www.mda.mil/system/system.html

[3] S. Sabatini and M. Tarantino, *Multifunction Array Radar - System Design and Analysis*. Artech House, 1994.

[4] M. Skolnik, *Introduction to Radar Systems*, 3rd ed. McGraw-Hill, 2001.

[5] S. Miranda, C. Baker, K. Woodbridge, and H. Griffiths, "Knowledge-based resource mangement for multifunction radar," in *IEEE Signal Processing Magazine*, 2006.

[6] B. Weir and T. Sokol, "Radar coordination and resource management in a distributed sensor network using emergent control," in *Proc. of SPIE*, vol. 7350, 2009.

[7] [Online]. Available: http://tinyurl.com/lqjeff2

[8] C.M.Fonseca and P. Fleming, "Genetic algorithms for multiobjective optimization: Formulation, discussion and generalization," in *Proc. 5th Int. Conf. Genetic Algorithms*, 1993, pp. 416–423.

[9] R. Saber and R. Murray, "Consensus and cooperation in networked multi-agent systems," in *Proceedings of the IEEE*, vol. 95, Jan 2007, pp. 215–223.

[10] W. Ren, R. Beard, and E. Atkins, "A survey of consensus problems in multi-agent coordination," *American Control Conference*, pp. 1859–1864, June 2005.

[11] W. Ren and R. Beard, "Consensus seeking in multi-agent systems under dynamically changing interaction topologies," in *IEEE Trans. Autom. Control*, vol. 50, May 2005, pp. 655–661.

[12] R. Saber and R. Murray, "Consensus problems in networks of agents with switching topology and time-delays," *IEEE Transactions on Automatic Control*, vol. 49, no. 9, September 2004.

[13] A. Hero and D. Cochran, "Sensor management: Past, present, and future," in *IEEE Sensors Journal*, vol. 11, no. 12, 2011, pp. 3064–3075.

[14] D. J. Kershaw and R. J. Evans, "Optimal waveform selection for tracking systems," in *IEEE Trans. Inform. Theory*, vol. 40, no. 5, Sep 1994, pp. 1536–1550.

[15] ——, "Waveform selective probabilistic data association," in *IEEE Trans. Aerosp. Electron. Syst.*, vol. 33, no. 4, Oct 1997, pp. 1180–1188.

[16] S. Sowelam and A. H. Tewfik, "Optimal waveform selection in range-doppler imaging," in *Proc. IEEE Int. Conf. Image Process*, Nov 1994, pp. 441–445.

[17] S. M. Sowelam and A. H. Tewfik, "Optimal waveform selection for radar target classification," in *Proc. IEEE Int. Conf. Image Process*, Oct 1997, pp. 476–479.

[18] S. Ghosh, J. Hansen, R. Rajkumar, and J. Lehoczky, "Integrated resource management and scheduling with multi-resource constraints," in *Proceedings of the 25th IEEE International Real-Time Systems Symposium*, 2004, pp. 12–22.

[19] A. Charlish, K. Woodbridge, and H. Griffiths, "Multi-target tracking control using continuous double auction parameter selection," in *Proc. of the 15th International Conf on Information Fusion*, 2012, pp. 1269–1276.

[20] N. Goodman, P. Venkata, and M. Neifeld, "Adaptive waveform design and sequential hypothesis testing for target recognition with active sensors," in *IEEE. J. Select. Topics Signal Process.*, vol. 1, no. 1, Jun 2007, pp. 105–113.

[21] S. Sira, Y. Li, A. Papandreou-Suppappola, D. Morrell, D. Cochran, and M. Rangaswamy, "Waveform-agile sensing for tracking," in *IEEE. Signal Process. Mag.*, vol. 26, no. 1, 2009 2009, pp. 53–64.

[22] A. Leshem, O. Naparstek, and A. Nehorai, "Information theoretic adaptive radar waveform design for multiple-extended targets," in *IEEE J. Select Topics Signal Process.*, vol. 1, no. 1, Jun 2007, pp. 42–55.

[23] A. Izquierdo-Fuente and J. Casar-Corredera, "Optimal radar pulse scheduling using a neural network," in *IEEE Int. Conf on Neural Networks*, vol. 7, 1994, pp. 4588–4591.

[24] V. Krishnamurthy and D. Djonin, "Optimal threshold policies for multivariate POMDPs in radar resource management," in *IEEE Trans. Signal Process.*, vol. 57, no. 10, Oct. 2009, pp. 3954–3969.

[25] J. Niño-Mora and S. Villar, "Multitarget tracking via restless bandit marginal productivity indices and kalman filter in discrete time," in *Joint 48th IEEE Conf. on Decision and Control and 28th Chinese Control Conf.*, Dec. 2009, pp. 2905–2909.

[26] B. F. L. Scala and B. Moran, "Optimal target tracking with restless bandits," in *Digital Signal Process.*, vol. 16, no. 5, 2006 2006, pp. 479–487.

[27] D. Khosla and J. Guillochon, "Distributed sensor resource management and planning," in *Proc. of SPIE on Signal Processing, Sensor Fusion, and Target Recognition*, vol. 6567, 2007.

[28] S. Sinno and D. Kreithen, "A constrained joint optimization approach to dynamic sensor configuration," in *Conf. Record of the 36th Asilomar Conf on Signals, Systems and Computers*, vol. 2, 2002, pp. 1179–1183.

[29] M. Kalandros and L. Pao, "Covariance control for multisensor systems," in *IEEE Transactions on Aerospace and Electronic Systems*, 2002, pp. 1138–1157.

[30] C. Kreucher, K. Kastella, and A. O. Hero, "Information based sensor management for multitarget tracking," in *Proc. of SPIE on Signal and Data Process. of Small Targets*, vol. 5204, 2003, pp. 480–489.

[31] A. Rényi, "On measures of entropy and information," in *Proc. 4th Berkeley Symp. Math. Stat. and Prob.*, vol. 1, 1961, pp. 547–561.

[32] C. Schumacher, P. Chandler, and S. Rasmussen, "Task allocation for wide area search munitions," in *Proceedings of the American Control Conference*, 2002, pp. 1917–1922.

[33] S. L. Smith and F. Bullo, "Monotonic target assignment for robotic networks," *IEEE Transactions on Automatic Control*, vol. 54, no. 9, pp. 2042–2057, 2009.

[34] K. J. Obermeyer, A. Ganguli, and F. Bullo, "A complete algorithm for searchlight scheduling," *International Journal of Computational Geometry and Applications*, vol. 21, no. 1, pp. 101–130, October 2011.

[35] P.-S. Kang and C.-G. Lee, "Coordinated search and track by multiple phased array radars," in *10th IEEE Real-Time and Embedded Technology and Applications Symposium*, no. 10. IEEE Computer Society, 2004, pp. 227–235.

[36] H. Lambert and D. Sinno, "Bioinspired resource management for multiple-sensor target tracking systems," M.I.T., Tech. Rep., 2011.

[37] Y. Mostofi and M. Malmirchegini, "Binary consensus over fading channels," in *IEEE Trans. on Signal Processing*, vol. 58, no. 12, 2010, pp. 6340–6353.

[38] D. R. Billetter, *Multifunction Array Radar*. Artech House, 1989.

[39] A. Charlish, "Autonomous agents for multi-function radar resource management," Ph.D. dissertation, Univ. College London, 2011.

[40] C. Scott, "The neyman-pearson criterion."

[41] M. Richards, *Fundamentals of Radar Signal Processing*. McGraw-Hill, New York, 2005.

[42] T. Jeffrey, *Phased Array Radar Design*. SciTech Publishing, Inc., 2009.

[43] T. W. Jeffrey, "Track quality estimation for multiple-target tracking radars," in *Proc. of 1989 Nation Radar Conf.*, 1989, pp. 76–79.

[44] M. Skolnik, *Radar Handbook*, 3rd ed. McGraw-Hill, 2008.

[45] C.Bacchus, D. Bedford, P. Dailey, S. Hill, I.Barford, J.Chung, R. Hazle, and M. Mihocka, "Digital array radar for ballistic missile defense and counter-stealth systems analysis and parameter tradeoff study," Naval Postgraduate School, Tech. Rep. SE-06-001, 2006.

[46] E. W. Weisstein. Solid angle. [Online]. Available: http://mathworld.wolfram.com/SolidAngle.html

[47] D. Bertsimas and J. Tsitsiklis, "Simulated annealing," *Statistical Science*, vol. 8, no. 1, pp. 10–15, 1993.

[48] A. Levitin, *Introduction to the Design and Analysis of Algorithms*, 3rd ed. Addison-Wesley, 2011.

[49] D. S. Hochbaum, "Complexity and algorithms for nonlinear optimization problems," *Annals of Operations Research*, vol. 153, no. 1, pp. 257–296, 2007.

[50] G. H. Sasaki and B. Hajek, "The time complexity of maximum matching by simulated annealing," *Journal of the ACM*, vol. 35, pp. 387–403, 1988.

[51] D. Mitra, F. Romeo, and A. Sangiovanni-Vincentelli, "Convergence and finite-time behavior of simmulated annealing," in *Advances in Applied Probability*, 1986, pp. 747–771.

[52] D. Henderson, S. Jacobson, and A. Johnson, *The theory and practice of simulated annealing.* Handbook of metaheuristics, 2003, pp. 287–319.

[53] A. Farina, B. Ristic, and D. Benvenuti, "Tracking a ballistic target: Comparison of several nonlinear filters," in *IEEE Transactions on Aerospace and Electronic Systems*, 2002, pp. 854–867.

[54] K. V. Ramachandra, *Kalman Filtering Techniquest for Radar Tracking.* Marcel Dekker, Inc., 2000.

[55] A. Farina, M. D. Gaudio, U. D'Elia, S. Immediata, and L. Ortenzi, "Detection and tracking of ballistic target," in *Proc. of the IEEE Radar Conf*, 2004, pp. 450–456.

[56] X. R. Li and V. P. Jilkov, "A survey of maneuvering target tracking - part ii: Ballistic target models," in *Proc. of SPIE Conf on Signal and Data Processing of Small Targets*, 2001.

[57] Y. Bar-Shalom, Ed., *Multitarget-Multisensor Tracking: Advanced Applications.* Artech House, 1990.

[58] S. S. Blackmann, *Multiple-Target Tracking with Radar Applications.* Artech House, 1986.

[59] D. Lerro and Y. Bar-Shalom, "Tracking with debiased consistent converted measurements versus ekf," in *IEEE Transactions on Aerospace and Electronic Systems*, 1993, pp. 1015–1022.

[60] J. Mingrone and M. L. Venuti, *Track Quality to Track Error Covariance*, Lockheed Martin Corporation, http://www.freepatentsonline.com/8052054.html, 2001.

[61] C. Godsil and G. Royle, *Algebraic Graph Theory.* Springer, 2001.

[62] N. Biggs, *Algebraic Graph Theory*, 2nd ed. Cambridge University Press, 1993.

[63] R. Diestel, *Graph Theory, Grad. Texts in Math.* Springer, 2005.

[64] N.J.Harvey, R. Ladner, L. Lovasz, and T. Tamir, "Semi-matchings for bipartite graphs and load balancing," in *Workshop of Algorithms and Data Structures*, 2003.

[65] K. Cai and H. Ishii, "Average consensus on general strongly connected digraphs," in *Proc. of the 28th American Control Conference (ACC)*, 2012, pp. 14–19.

[66] ——, "Quantized consensus and averaging on gossip digraphs," in *IEEE Trans. Autom. Control*, vol. 56, no. 9, Sept 2011, pp. 2087–2100.

[67] M. Fewell, "Area of common overlap of three circles," Defence Science and Technology Organisation, P.O. Box 1500, Edinburgh, SA 5111, Australia, Tech. Rep., October 2006.

[68] Army Technology. Arrow 2, Israel. [Online]. Available: http://www.army-technology.com/projects/arrow2

[69] A. Konak, D. Coit, and A. E. Smith, "Multi-objective optimization using genetic algorithms: A tutorial," in *Reliability Engineering and System Safety*, vol. 91, 2006, pp. 992–1007.

[70] I. Kim and O. de Weck, "Adaptive weighted-sum method for bi-objective optimization: Pareto front generation," in *AIAA/ASME/ASCE/AHS/ASC Structures, Structural Dynamics, and Materials Conference*, 2004.

[71] Y. Mostofi, "Binary consensus with gaussian communication noise: A probabilistic approach," in *Proc of the 46th IEEE Conf on Decision and Control*, 2007, pp. 2528–2533.

[72] S. Kazarlis, A. Bakistzis, and V. Petridis, "A genetic algorithm solution to the unit commitment problem," in *IEEE Trans on Power Systems*, 1996.

[73] D. B. Fogel, "Evolving articifical intelligence," Ph.D. dissertation, San Diego: Univ. of California, 1992.

[74] D. E. Goldberg, *Genetic Algorithms in Search, Optimization, and Machine Learning.* Reading/Mass.: Addison Wesley, 1989.

[75] G. Rudolph, "Convergence analysis of canonical genetic algorithms," *IEEE Trans. Neural Networks*, vol. 5, no. 1, pp. 96–101, 1994.

[76] R. Haupt and S. Haupt, *Practical Genetic Algorithms.* John Wiley and Sons, Inc., 2004.

[77] Y. Yuan and Y. Mostofi, "Impact of link qualities and network topology on binary consensus," in *Proc. of the 28th American Control Conference (ACC)*, June 2009, pp. 1821–1826.

[78] B. Skylar, *Digital Communications*, 2nd ed. Prentice Hall, 2001.

[79] R. Corp. (2002) Cruise missile and ballistic missile defense. [Online]. Available: http://www.rand.org/content/dam/rand/pubs/monograph_reports/MR1449/MR1449.ch3.pdf

[80] W. Gilson, "Minimum power requirements of tracking," in *IEEE Radar Conference*, 1990, pp. 417–421.

[81] S. L. Coetzee, K. Woodbridge, and C. Baker, "Multifunction radar resource management using tracking optimisation," in *Proc. Int. Conf. RADAR*, Sept. 2003, pp. 578–583.

[82] Y.-H. Jung and S.-M. Hong, "Modeling and parameter optimization of agile beam radar tracking," in *IEEE Transactions on Aerospace and Electronic Systems*, vol. 39, no. 1. Aerospace, 2003, pp. 13–33.

[83] Y. Bar-Shalom and H. Chen, "Multisensor track-to-track association for tracks with dependent errors," in *Journal of Advances in Information Fusion*, vol. 1, no. 1, 2006, pp. 3–14.

[84] S. R. Lay, *Analysis With an Introduction to Proof*, 2nd ed. Prentice Hall, 1990.